Chapter 21
Simple Quantum Systems

In this chapter we study simple quantum systems. A particle in a one-dimensional potential $V(x)$ is described by a wave packet which is a solution of the partial differential equation [232]

$$\mathrm{i}\hbar\frac{\partial}{\partial t}\psi(x) = H\psi(x) = -\frac{\hbar^2}{2m}\frac{\partial^2}{\partial x^2}\psi(x) + V(x)\psi(x). \tag{21.1}$$

We discuss two approaches to discretize the second derivative. Finite differences are simple to use but their dispersion deviates largely from the exact relation, except high order differences are used. Pseudo-spectral methods evaluate the kinetic energy part in Fourier space and are much more accurate. The time evolution operator can be approximated by rational expressions like Cauchy's form which corresponds to the Crank-Nicholson method. These schemes are unitary but involve time consuming matrix inversions. Multistep differencing schemes have comparable accuracy but are explicit methods. Best known is second order differencing. Split operator methods approximate the time evolution operator by a product. In combination with finite differences for the kinetic energy this leads to the method of real-space product formula which can applied to wavefunctions with more than one component, for instance to study transitions between states. In a computer experiment we simulate a one-dimensional wave packet in a potential with one or two minima.

Few-state systems are described with a small set of basis states. Especially the quantum mechanical two-level system is often used as a simple model for the transition between an initial and a final state due to an external perturbation.[1] Its wavefunction has two components

$$|\psi\rangle = \begin{pmatrix} C_1 \\ C_2 \end{pmatrix} \tag{21.2}$$

which satisfy two coupled ordinary differential equations for the amplitudes $C_{1,2}$ of the two states

[1] For instance collisions or the electromagnetic radiation field.

P.O.J. Scherer, *Computational Physics*, Graduate Texts in Physics,
DOI 10.1007/978-3-319-00401-3_21,

$$\mathrm{i}\hbar\frac{\mathrm{d}}{\mathrm{d}t}\begin{pmatrix} C_1 \\ C_2 \end{pmatrix} = \begin{pmatrix} H_{11} & H_{12} \\ H_{21} & H_{22} \end{pmatrix}\begin{pmatrix} C_1 \\ C_2 \end{pmatrix}. \tag{21.3}$$

In several computer experiments we study a two-state system in an oscillating field, a three-state system as a model for superexchange, the Landau-Zener model for curve-crossing and the ladder model for exponential decay. The density matrix formalism is used to describe a dissipative two-state system in analogy to the Bloch equations for nuclear magnetic resonance. In computer experiments we study the resonance line and the effects of saturation and power broadening. Finally we simulate the generation of a coherent superposition state or a spin flip by applying pulses of suitable duration. This is also discussed in connection with the manipulation of a qubit represented by a single spin.

21.1 Pure and Mixed Quantum States

Whereas pure states of a quantum system are described by a wavefunction, mixed states are described by a density matrix. Mixed states appear if the exact quantum state is unknown, for instance for a statistical ensemble of quantum states, a system with uncertain preparation history, or if the system is entangled with another system. A mixed state is different from a superposition state. For instance, the superposition

$$|\psi\rangle = C_0|\psi_0\rangle + C_1|\psi_1\rangle \tag{21.4}$$

of the two states $|\psi_0\rangle$ and $|\psi_1\rangle$ is a pure state, which can be described by the density operator

$$\begin{aligned} |\psi\rangle\langle\psi| = {} & |C_0|^2|\psi_0\rangle\langle\psi_0| + |C_1|^2|\psi_1\rangle\langle\psi_1| \\ & + C_0C_1^*|\psi_0\rangle\langle\psi_1| + C_0^*C_1|\psi_1\rangle\langle\psi_0| \end{aligned} \tag{21.5}$$

whereas the density operator

$$\rho = p_0|\psi_0\rangle\langle\psi_0| + p_1|\psi_1\rangle\langle\psi_1| \tag{21.6}$$

describes the mixed state of a system which is in the pure state $|\psi_0\rangle$ with probability p_0 and in the state $|\psi_1\rangle$ with probability $p_1 = 1 - p_0$. The expectation value of an operator A is in the first case

$$\begin{aligned} \langle A\rangle = \langle\psi|A|\psi\rangle = {} & |C_0|^2\langle\psi_0|A|\psi_0\rangle + |C_1|^2\langle\psi_1 A|\psi_1\rangle \\ & + C_0C_1^*\langle\psi_1|A|\psi_0\rangle + C_0^*C_1\langle\psi_0|A|\psi_1\rangle \end{aligned} \tag{21.7}$$

and in the second case

$$\langle A\rangle = p_0\langle\psi_0|A|\psi_0\rangle + p_1\langle\psi_1|A|\psi_1\rangle. \tag{21.8}$$

Both can be written in the form

$$\langle A\rangle = \mathrm{tr}(\rho A). \tag{21.9}$$

21.1.1 Wavefunctions

The time evolution of a quantum system is governed by the time dependent Schrödinger equation [230]

$$\mathrm{i}\hbar\frac{\partial}{\partial t}|\psi\rangle = H|\psi\rangle \tag{21.10}$$

for the wavefunction ψ. The brackets indicate that $|\psi\rangle$ is a vector in an abstract Hilbert space [122]. Vectors can be added

$$|\psi\rangle = |\psi_1\rangle + |\psi_2\rangle = |\psi_1 + \psi_2\rangle \tag{21.11}$$

and can be multiplied with a complex number

$$|\psi\rangle = \lambda|\psi_1\rangle = |\lambda\psi_1\rangle. \tag{21.12}$$

Finally a complex valued scalar product of two vectors is defined[2]

$$C = \langle\psi_1|\psi_2\rangle \tag{21.13}$$

which has the properties

$$\langle\psi_1|\psi_2\rangle = \langle\psi_2|\psi_1\rangle^* \tag{21.14}$$

$$\langle\psi_1|\lambda\psi_2\rangle = \lambda\langle\psi_1|\psi_2\rangle = \left\langle\lambda^*\psi_1\middle|\psi_2\right\rangle \tag{21.15}$$

$$\langle\psi|\psi_1 + \psi_2\rangle = \langle\psi|\psi_1\rangle + \langle\psi|\psi_2\rangle \tag{21.16}$$

$$\langle\psi_1 + \psi_2|\psi\rangle = \langle\psi_1|\psi\rangle + \langle\psi_2|\psi\rangle. \tag{21.17}$$

21.1.2 Density Matrix for an Ensemble of Systems

Consider a thermal ensemble of systems. Their wave functions are expanded with respect to basis functions $|\psi_s\rangle$ as

$$|\psi\rangle = \sum_s C_s|\psi_s\rangle. \tag{21.18}$$

The ensemble average of an operator A is given by

$$\overline{\langle A\rangle} = \overline{\langle\psi A\psi\rangle} = \overline{\left\langle\sum_{s,s'} C_s^*\psi_s A C_{s'}\psi_{s'}\right\rangle} \tag{21.19}$$

$$= \sum_{s,s'}\overline{C_s^* C_{s'}}A_{ss'} = \mathrm{tr}(\rho A) \tag{21.20}$$

[2] If, for instance the wavefunction depends on the coordinates of N particles, the scalar product is defined by $\langle\psi_n|\psi_{n'}\rangle = \int d^3r_1\cdots d^3r_N\,\psi_n^*(r_1\cdots r_N)\psi_{n'}(r_1\cdots r_N)$.

with the density matrix

$$\rho_{s's} = \sum_{s,s'} \overline{C_s^* C_{s'}}. \tag{21.21}$$

The wave function of an N-state system is a linear combination

$$|\psi\rangle = C_1|\psi_1\rangle + C_2|\psi_2\rangle + \cdots + C_N|\psi_N\rangle. \tag{21.22}$$

The diagonal elements of the density matrix are the occupation probabilities

$$\rho_{11} = \overline{|C_1|^2} \qquad \rho_{22} = \overline{|C_2|^2} \cdots \qquad \rho_{NN} = \overline{|C_N|^2} \tag{21.23}$$

and the nondiagonal elements measure the correlation of two states[3]

$$\rho_{12} = \rho_{21}^* = \overline{C_2^* C_1}, \quad \ldots. \tag{21.24}$$

21.1.3 Time Evolution of the Density Matrix

The expansion coefficients of

$$|\psi\rangle = \sum_s C_s|\psi_s\rangle \tag{21.25}$$

can be obtained from the scalar product

$$C_s = \langle\psi_s|\psi\rangle. \tag{21.26}$$

Hence we have

$$C_s^* C_{s'} = \langle\psi|\psi_s\rangle\langle\psi_{s'}|\psi\rangle = \langle\psi_{s'}|\psi\rangle\langle\psi|\psi_s\rangle \tag{21.27}$$

which can be considered to be the s', s matrix element of the projection operator $|\psi\rangle\langle\psi|$

$$C_s^* C_{s'} = \big(|\psi\rangle\langle\psi|\big)_{s's}. \tag{21.28}$$

The thermal average of $|\psi\rangle\langle\psi|$ is the statistical operator

$$\rho = \overline{|\psi\rangle\langle\psi|} \tag{21.29}$$

which is represented by the density matrix with respect to the basis functions $|\psi_s\rangle$

$$\rho_{s's} = \overline{|\psi\rangle\langle\psi|}_{s's} = \overline{C_s^* C_{s'}}. \tag{21.30}$$

From the Schrödinger equation

$$i\hbar|\dot{\psi}\rangle = H|\psi\rangle \tag{21.31}$$

we find

[3] They are often called the "coherence" of the two states.

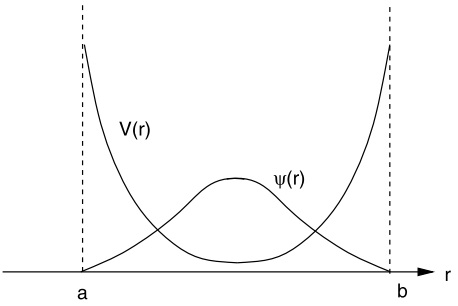

Fig. 21.1 Potential well

$$-i\hbar\langle\dot{\psi}| = \langle H\psi| = \langle\psi|H \tag{21.32}$$

and hence

$$i\hbar\dot{\rho} = i\hbar\big(\overline{|\dot{\psi}\rangle\langle\psi|} + \overline{|\psi\rangle\langle\dot{\psi}|}\big) = \overline{|H\psi\rangle\langle\psi|} - \overline{|\psi\rangle\langle H\psi|}. \tag{21.33}$$

Since the Hamiltonian H is identical for all members of the ensemble we end up with the Liouville-von Neumann equation

$$i\hbar\dot{\rho} = H\rho - \rho H = [H, \rho]. \tag{21.34}$$

With respect to a finite basis this becomes explicitly:

$$i\hbar\dot{\rho}_{ii} = \sum_j H_{ij}\rho_{ji} - \rho_{ij}H_{ji} = \sum_{j\neq i} H_{ij}\rho_{ji} - \rho_{ij}H_{ji} \tag{21.35}$$

$$\begin{aligned} i\hbar\dot{\rho}_{ik} &= \sum_j H_{ij}\rho_{jk} - \rho_{ij}H_{jk} \\ &= (H_{ii} - H_{kk})\rho_{ik} + H_{ik}(\rho_{kk} - \rho_{ii}) + \sum_{j\neq i,k}(H_{ij}\rho_{jk} - \rho_{ij}H_{jk}). \end{aligned} \tag{21.36}$$

21.2 Wave Packet Motion in One Dimension

A quantum mechanical particle with mass m_p in a one-dimensional potential $V(x)$ is described by a complex valued wavefunction $\psi(x)$ (Fig. 21.1). We assume that the wavefunction is negligible outside an interval $[a, b]$. This is the case for a particle bound in a potential well i.e. a deep enough minimum of the potential or for a wave-packet with finite width far from the boundaries. Then the calculation can be restricted to the finite interval $[a, b]$ by applying the boundary condition

$$\psi(x) = 0 \quad \text{for } x \leq a \text{ or } x \geq b \tag{21.37}$$

or, if reflections at the boundary should be suppressed, transparent boundary conditions [9].

All observables (quantities which can be measured) of the particle are expectation values with respect to the wavefunction, for instance its average position is

$$\langle x \rangle = \big\langle \psi(x) x \psi(x) \big\rangle = \int_a^b dx\, \psi^*(x) x \psi(x). \tag{21.38}$$

The probability of finding the particle at the position x_0 is given by

$$P(x = x_0) = \big|\psi(x_0)\big|^2. \tag{21.39}$$

For time independent potential $V(x)$ the Schrödinger equation

$$\mathrm{i}\hbar\dot{\psi} = H\psi = \left(-\frac{\hbar^2}{2m_p}\frac{\partial^2}{\partial x^2} + V(x)\right)\psi \tag{21.40}$$

can be formally solved by

$$\psi(t) = U(t, t_0)\psi(t_0) = \exp\left\{-\frac{\mathrm{i}(t - t_0)}{\hbar} H\right\}\psi(t_0). \tag{21.41}$$

If the potential is time dependent, the more general formal solution is

$$\begin{aligned}\psi(t) = U(t, t_0)\psi(t_0) &= \hat{T}_t \exp\left\{-\frac{\mathrm{i}}{\hbar}\int_{t_0}^t H(\tau)\, d\tau\right\}\psi(t_0) \\ &= \sum_{n=0}^{\infty} \frac{1}{n!}\left(\frac{-\mathrm{i}}{\hbar}\right)^n \int_{t_0}^t dt_1 \int_{t_0}^t dt_2 \ldots \int_{t_0}^t dt_n\, \hat{T}_t\big\{H(t_1)H(t_2)\ldots H(t_n)\big\}\end{aligned} \tag{21.42}$$

where $\hat{T}_t$ denotes the time ordering operator. The simplest approach is to divide the time interval $0 \ldots t$ into a sequence of smaller steps

$$U(t, t_0) = U(t, t_{N-1}) \ldots U(t_2, t_1) U(t_1, t_0) \tag{21.43}$$

and to neglect the variation of the Hamiltonian during the small interval $\Delta t = t_{n+1} - t_n$ [158]

$$U(t_{n+1}, t_n) = \exp\left\{-\frac{\mathrm{i}\Delta t}{\hbar} H(t_n)\right\}. \tag{21.44}$$

21.2.1 Discretization of the Kinetic Energy

The kinetic energy

$$T\psi(x) = -\frac{\hbar^2}{2m_p}\frac{\partial^2}{\partial x^2}\psi(x) \tag{21.45}$$

is a nonlocal operator in real space. It is most efficiently evaluated in Fourier space where it becomes diagonal

$$\mathcal{F}[T\psi](k) = \frac{\hbar^2 k^2}{2m_p}\mathcal{F}[\psi](k). \tag{21.46}$$

21.2.1.1 Pseudo-spectral Methods

The potential energy is diagonal in real space. Therefore, pseudo-spectral (Sect. 11.5.1) methods [93] use a Fast Fourier Transform algorithm (Sect. 7.3.2) to switch between real space and Fourier space. They calculate the action of the Hamiltonian on the wavefunction according to

$$H\psi(x) = V(x)\psi(x) + \mathcal{F}^{-1}\left[\frac{\hbar^2 k^2}{2m_p}\mathcal{F}[\psi](k)\right]. \tag{21.47}$$

21.2.1.2 Finite Difference Methods

In real space, the kinetic energy operator can be approximated by finite differences on a grid, like the simple 3-point expression (3.31)

$$-\frac{\hbar^2}{2m_p}\frac{\psi^n_{m+1} + \psi^n_{m-1} - 2\psi^n_m}{\Delta x^2} + O\left(\Delta x^2\right) \tag{21.48}$$

or higher order expressions (3.33)

$$-\frac{\hbar^2}{2m_p}\frac{-\psi^n_{m+2} + 16\psi^n_{m+1} - 30\psi^n_m + 16\psi^n_{m-1} - \psi^n_{m-2}}{12\Delta x^2} + O\left(\Delta x^4\right) \tag{21.49}$$

$$-\frac{\hbar^2}{2m_p}\frac{1}{\Delta x^2}\left(\frac{1}{90}\psi^n_{m+3} - \frac{3}{20}\psi^n_{m+2} + \frac{3}{2}\psi^n_{m+1} - \frac{49}{18}\psi^n_m + \frac{3}{2}\psi^n_{m-1} - \frac{3}{20}\psi^n_{m-2} + \frac{1}{90}\psi^n_{m-3}\right) + O\left(\Delta x^6\right) \tag{21.50}$$

etc. [94]. However, finite differences inherently lead to deviations of the dispersion relation from (21.46). Inserting $\psi_m = \mathrm{e}^{\mathrm{i}km\Delta x}$ we find

$$E(k) = \frac{\hbar^2}{2m_p}\frac{2(1-\cos(k\Delta x))}{\Delta x^2} \tag{21.51}$$

for the 3-point expression (21.48),

$$E(k) = \frac{\hbar^2}{2m_p}\frac{15 - 16\cos(k\Delta x) + \cos(2k\Delta x)}{6\Delta x^2} \tag{21.52}$$

for the 5-point expression (21.49) and

$$\frac{\hbar^2}{2m_p}\frac{1}{\Delta x^2}\left(\frac{49}{18} - 3\cos(k\Delta x) + \frac{3}{10}\cos(2k\Delta x) - \frac{1}{45}\cos(3k\Delta x)\right) \tag{21.53}$$

for the 7-point expression (21.50). Even the 7-point expression shows large deviations for k-values approaching $k_{\max} = \pi/\Delta x$ (Fig. 21.2). However, it has been shown that not very high orders are necessary to achieve the numerical accuracy of the pseudo-spectral Fourier method [113] and that finite difference methods may be even more efficient in certain applications [114].

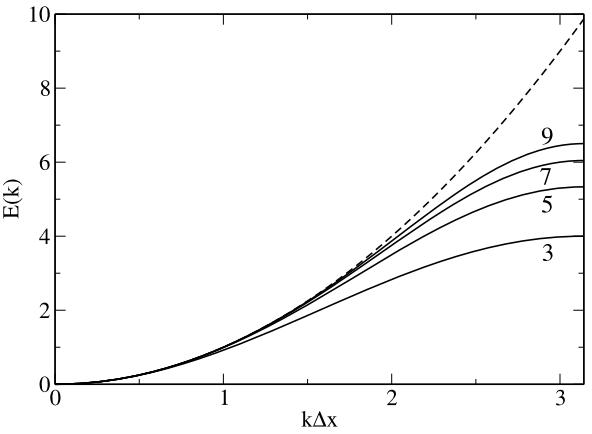

Fig. 21.2 (Dispersion of finite difference expressions) The dispersion relation of finite difference expressions of increasing order ((21.48), (21.49), (21.50) and the symmetric 9-point approximation [94]) are compared to the exact dispersion (21.46) of a free particle (*dashed curve*)

21.2.2 Time Evolution

A number of methods have been proposed [7, 51, 158, 278] to approximate the short time propagator (21.44). Unitarity is a desirable property since it guaranties stability and norm conservation even for large time steps. However, depending on the application, small deviations from unitarity may be acceptable in return for higher efficiency. The Crank-Nicolson (CN) method [104, 172, 173] is one of the first methods which have been applied to the time dependent Schrödinger equation. It is a unitary but implicit method and needs the inversion of a matrix which can become cumbersome in two or more dimensions or if high precision is required. Multistep methods [131, 132], especially second order [10] differencing (SOD) are explicit but only conditionally stable and put limits to the time interval Δt. Split operator methods (SPO) approximate the propagator by a unitary product of operators [14, 67, 68]. They are explicit and easy to implement. The real-space split-operator method has been applied to more complex problems like a molecule in a laser field [61]. Polynomial approximations, especially the Chebishev expansion [53, 248], have very high accuracy and allow for large time steps, if the Hamiltonian is time independent. However, they do not provide intermediate results and need many applications of the Hamiltonian. The short time iterative Lanczos (SIL) method [57, 153, 197] is very useful also for time dependent Hamiltonians. Even more sophisticated methods using finite elements and the discrete variable representation are presented for instance in [4, 226]. In the following we discuss three methods (CN, SOD, SPO) which are easy to implement and well suited to solve the time dependent Schrödinger equation for a mass point moving in a one-dimensional potential.

21.2.2.1 Rational Approximation

Taking the first terms of the Taylor expansion

$$U(t_{n+1}, t_n) = \exp\left\{-\frac{\mathrm{i}\Delta t}{\hbar} H\right\} = 1 - \frac{\mathrm{i}\Delta t}{\hbar} H + \cdots \tag{21.54}$$

corresponds to a simple explicit Euler step

$$\psi(t_{n+1}) = \left(1 - \frac{\mathrm{i}\Delta t}{\hbar} H\right)\psi(t_n). \tag{21.55}$$

From the real eigenvalues E of the Hamiltonian we find the eigenvalues of the explicit method

$$\lambda = 1 - \frac{\mathrm{i}\Delta t}{\hbar} E \tag{21.56}$$

which all have absolute values

$$|\lambda| = \sqrt{1 + \frac{\Delta t^2 E^2}{\hbar^2}} > 1. \tag{21.57}$$

Hence the explicit method is not stable.

Expansion of the inverse time evolution operator

$$U(t_n, t_{n+1}) = U(t_{n+1}, t_n)^{-1} = \exp\left\{+\frac{\mathrm{i}\Delta t}{\hbar} H\right\} = 1 + \frac{\mathrm{i}\Delta t}{\hbar} H + \cdots$$

leads to the implicit method

$$\psi(t_{n+1}) = \psi(t_n) - \frac{\mathrm{i}\Delta t}{\hbar} H\psi(t_{n+1}) \tag{21.58}$$

which can be rearranged as

$$\psi(t_{n+1}) = \left(1 + \frac{\mathrm{i}\Delta t}{\hbar} H\right)^{-1} \psi(t_n). \tag{21.59}$$

Now all eigenvalues have absolute values < 1. This method is stable but the norm of the wave function is not conserved. Combination of implicit and explicit method gives a method [172, 173] similar to the Crank-Nicolson method for the diffusion equation (Sect. 19.2.3)

$$\psi(t_{n+1}) - \psi(t_n) = -\frac{\mathrm{i}\Delta t}{\hbar} H\left(\frac{\psi(t_{n+1})}{2} + \frac{\psi(t_n)}{2}\right). \tag{21.60}$$

This equation can be solved for the new value of the wavefunction

$$\psi(t_{n+1}) = \left(1 + \mathrm{i}\frac{\Delta t}{2\hbar} H\right)^{-1} \left(1 - \mathrm{i}\frac{\Delta t}{2\hbar} H\right)\psi(t_n) \tag{21.61}$$

which corresponds to a rational approximation[4] of the time evolution operator (Cayley's form)

[4] The Padé approximation (Sect. 2.4.1) of order [1, 1].

$$U(t_{n+1},t_n)\approx\frac{1-\mathrm{i}\frac{\Delta t}{2\hbar}H}{1+\mathrm{i}\frac{\Delta t}{2\hbar}H}. \tag{21.62}$$

The eigenvalues of (21.62) all have an absolute value of

$$|\lambda|=\left|\left(1+\mathrm{i}\frac{E\Delta t}{2\hbar}\right)^{-1}\left(1-\mathrm{i}\frac{E\Delta t}{2\hbar}\right)\right|=\frac{\sqrt{1+\frac{E^2\Delta t^2}{4\hbar^2}}}{\sqrt{1+\frac{E^2\Delta t^2}{4\hbar^2}}}=1. \tag{21.63}$$

It is obviously a unitary operator and conserves the norm of the wavefunction since

$$\left(\frac{1-\mathrm{i}\frac{\Delta t}{2\hbar}H}{1+\mathrm{i}\frac{\Delta t}{2\hbar}H}\right)^{\dagger}\left(\frac{1-\mathrm{i}\frac{\Delta t}{2\hbar}H}{1+\mathrm{i}\frac{\Delta t}{2\hbar}H}\right)=\left(\frac{1+\mathrm{i}\frac{\Delta t}{2\hbar}H}{1-\mathrm{i}\frac{\Delta t}{2\hbar}H}\right)\left(\frac{1-\mathrm{i}\frac{\Delta t}{2\hbar}H}{1+\mathrm{i}\frac{\Delta t}{2\hbar}H}\right)=1 \tag{21.64}$$

as H is Hermitian $H^{\dagger}=H$ and $(1+\mathrm{i}\frac{\Delta t}{2\hbar}H)$ and $(1-\mathrm{i}\frac{\Delta t}{2\hbar}H)$ are commuting operators. From the Taylor series we find the error order

$$\begin{aligned}&\left(1+\mathrm{i}\frac{\Delta t}{2\hbar}H\right)^{-1}\left(1-\mathrm{i}\frac{\Delta t}{2\hbar}H\right)\\&=\left(1-\mathrm{i}\frac{\Delta t}{2\hbar}H-\frac{\Delta t^2}{4\hbar^2}H^2+\cdots\right)\left(1-\mathrm{i}\frac{\Delta t}{2\hbar}H\right)\\&=1-\frac{\mathrm{i}\Delta t}{\hbar}H-\frac{\Delta t^2}{2\hbar^2}H^2+\cdots=\exp\left(-\frac{i\Delta t}{\hbar}H\right)+O\left(\Delta t^3\right).\end{aligned} \tag{21.65}$$

For practical application we rewrite [149]

$$\begin{aligned}\left(1+\mathrm{i}\frac{\Delta t}{2\hbar}H\right)^{-1}\left(1-\mathrm{i}\frac{\Delta t}{2\hbar}H\right)&=\left(1+\mathrm{i}\frac{\Delta t}{2\hbar}H\right)^{-1}\left(-1-\mathrm{i}\frac{\Delta t}{2\hbar}H+2\right)\\&=-1+2\left(1+\mathrm{i}\frac{\Delta t}{2\hbar}H\right)^{-1}\end{aligned} \tag{21.66}$$

hence

$$\psi(t_{n+1})=2\left(1+\mathrm{i}\frac{\Delta t}{2\hbar}H\right)^{-1}\psi(t_n)-\psi(t_n)=2\chi-\psi(t_n). \tag{21.67}$$

$\psi(t_{n+1})$ is obtained in two steps. First we have to solve

$$\left(1+\mathrm{i}\frac{\Delta t}{2\hbar}H\right)\chi=\psi(t_n). \tag{21.68}$$

Then $\psi(t_{n+1})$ is given by

$$\psi(t_{n+1})=2\chi-\psi(t_n). \tag{21.69}$$

We use the finite difference method (Sect. 11.2) on the grid

$$x_m=m\Delta x\quad m=0\cdots M\quad \psi_m^n=\psi(t_n,x_m) \tag{21.70}$$

and approximate the second derivative by

$$\frac{\partial^2}{\partial x^2}\psi(t_n, x_m) = \frac{\psi^n_{m+1} + \psi^n_{m-1} - 2\psi^n_m}{\Delta x^2} + O\left(\Delta x^2\right). \tag{21.71}$$

Equation (21.68) then becomes a system of linear equations

$$A \begin{bmatrix} \chi_0 \\ \chi_1 \\ \vdots \\ \chi_M \end{bmatrix} = \begin{bmatrix} \psi^n_0 \\ \psi^n_1 \\ \vdots \\ \psi^n_M \end{bmatrix} \tag{21.72}$$

with a tridiagonal matrix

$$A = 1 - \mathrm{i}\frac{\hbar\Delta t}{4m_p\Delta x^2}\begin{pmatrix} 2 & -1 & & \\ -1 & 2 & \ddots & \\ & \ddots & \ddots & -1 \\ & & -1 & 2 \end{pmatrix} + \mathrm{i}\frac{\Delta t}{2\hbar}\begin{pmatrix} V_0 & & & \\ & V_1 & & \\ & & \ddots & \\ & & & V_M \end{pmatrix}. \tag{21.73}$$

The second step (21.69) becomes

$$\begin{bmatrix} \psi^{n+1}_0 \\ \psi^{n+1}_1 \\ \vdots \\ \psi^{n+1}_M \end{bmatrix} = 2\begin{bmatrix} \chi_0 \\ \chi_1 \\ \vdots \\ \chi_M \end{bmatrix} - \begin{bmatrix} \psi^n_0 \\ \psi^n_1 \\ \vdots \\ \psi^n_M \end{bmatrix}. \tag{21.74}$$

Inserting a plane wave

$$\psi = \mathrm{e}^{\mathrm{i}(kx-\omega t)} \tag{21.75}$$

we obtain the dispersion relation (Fig. 21.3)

$$\frac{2}{\Delta t}\tan(\omega\Delta t/2) = \frac{\hbar}{2m_p}\left(\frac{2}{\Delta x}\sin\frac{k\Delta x}{2}\right)^2 \tag{21.76}$$

which we rewrite as

$$\omega\Delta t = 2\arctan\left[\frac{2\alpha}{\pi^2}\sin^2\frac{k\Delta x}{\pi}\frac{\pi}{2}\right] \tag{21.77}$$

with the dimensionless parameter

$$\alpha = \frac{\pi^2\hbar\Delta t}{2m_p\Delta x^2}. \tag{21.78}$$

For time independent potentials the accuracy of this method can be improved systematically [261] by using higher order finite differences for the spatial derivative (Sect. 21.2.1.2) and a higher order Padé approximation (Sect. 2.4.1) of order $[M, M]$ for the exponential function

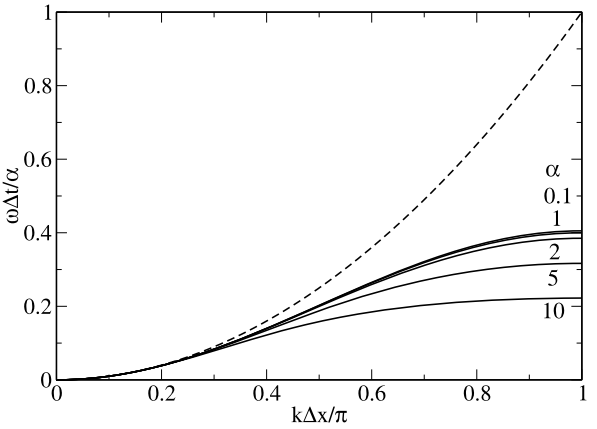

Fig. 21.3 (Dispersion of the Crank-Nicolson method) The dispersion relation of the Crank-Nicolson method (21.95) deviates largely from the exact dispersion (21.98), even for small values of the stability parameter α. The scaled frequency $\omega\Delta t/\alpha$ is shown as a function of $k\Delta x/\pi$ for $\alpha = 0.1, 1, 2, 5, 10$ (*solid curves*) and compared with the exact relation of a free particle $\omega\Delta t/\alpha = (k\Delta x/\pi)^2$ (*dashed curve*)

$$\mathrm{e}^z = \prod_{s=1}^{M} \frac{1 - z/z_s^{(M)}}{1 + z/z_s^{(M)*}} + O\left(z^{2M+1}\right) \tag{21.79}$$

to approximate the time evolution operator

$$\exp\left(-\frac{\mathrm{i}\Delta t}{\hbar} H\right) = \prod_{s=1}^{M} \frac{1 - (i\,\Delta t\, H/\hbar)/z_s^{(M)}}{1 + (i\,\Delta t\, H/\hbar)/z_s^{*(M)}} + O\left((\Delta t)^{2M+1}\right). \tag{21.80}$$

However, the matrix inversion can become very time consuming in two or more dimensions.

21.2.2.2 Second Order Differencing

Explicit methods avoid the matrix inversion. The method of second order differencing [10] takes the difference of forward and backward step

$$\psi(t_{n-1}) = U(t_{n-1}, t_n)\psi(t_n) \tag{21.81}$$

$$\psi(t_{n+1}) = U(t_{n+1}, t_n)\psi(t_n) \tag{21.82}$$

to obtain the explicit two-step algorithm

$$\psi(t_{n+1}) = \psi(t_{n-1}) + \left[U(t_{n+1}, t_n) - U^{-1}(t_n, t_{n-1})\right]\psi(t_n). \tag{21.83}$$

The first terms of the Taylor series give the approximation

$$\psi(t_{n+1}) = \psi(t_{n-1}) - 2\frac{\mathrm{i}\Delta t}{\hbar} H\psi(t_n) + O\left((\Delta t)^3\right) \tag{21.84}$$

which can also be obtained from the second order approximation of the time derivative [150]

$$H\psi = \mathrm{i}\hbar\frac{\partial}{\partial t}\psi = \frac{\psi(t+\Delta t)-\psi(t-\Delta t)}{2\Delta t}. \tag{21.85}$$

This two-step algorithm can be formulated as a discrete mapping

$$\begin{pmatrix}\psi(t_{n+1})\\ \psi(t_n)\end{pmatrix} = \begin{pmatrix}-2\frac{\mathrm{i}\Delta t}{\hbar}H & 1\\ 1 & 0\end{pmatrix}\begin{pmatrix}\psi(t_n)\\ \psi(t_{n-1})\end{pmatrix} \tag{21.86}$$

with eigenvalues

$$\lambda = -\frac{\mathrm{i}E_s\Delta t}{\hbar} \pm \sqrt{1-\frac{E_s^2\Delta t^2}{\hbar^2}}. \tag{21.87}$$

For sufficiently small time step [158]

$$\Delta t < \frac{\hbar}{\max|E_s|} \tag{21.88}$$

the square root is real,

$$|\lambda|^2 = \frac{E_s^2\Delta t^2}{\hbar^2} + \left(1-\frac{E_s^2\Delta t^2}{\hbar^2}\right) = 1 \tag{21.89}$$

and the method is conditionally stable and has the same error order as the Crank-Nicolson method (Sect. 21.2.2.1). Its big advantage is that it is an explicit method and does not involve matrix inversions. Generalization to higher order multistep differencing schemes is straightforward [131]. The method conserves [150] the quantities $\Re\langle\psi(t+\Delta t)|\psi(t)\rangle$ and $\Re\langle\psi(t+\Delta t)|H|\psi(t)\rangle$ but is not strictly unitary [10]. Consider a pair of wavefunctions at times t_0 and t_1 which obey the exact time evolution

$$\psi(t_1) = \exp\left\{-\frac{\mathrm{i}\Delta t}{\hbar}H\right\}\psi(t_0) \tag{21.90}$$

and apply (21.84) to obtain

$$\psi(t_2) = \left[1-2\frac{\mathrm{i}\Delta t}{\hbar}H\exp\left\{-\frac{\mathrm{i}\Delta t}{\hbar}H\right\}\right]\psi(t_0) \tag{21.91}$$

which can be written as

$$\psi(t_2) = \mathcal{L}\,\psi(t_0) \tag{21.92}$$

where the time evolution operator L obeys

$$\begin{aligned}\mathcal{L}^\dagger\mathcal{L} &= \left[1+2\frac{\mathrm{i}\Delta t}{\hbar}H\exp\left\{+\frac{\mathrm{i}\Delta t}{\hbar}H\right\}\right]\left[1-2\frac{\mathrm{i}\Delta t}{\hbar}H\exp\left\{-\frac{\mathrm{i}\Delta t}{\hbar}H\right\}\right]\\ &= 1-4\frac{\Delta t}{\hbar}H\sin\left\{\frac{\Delta t}{\hbar}H\right\}+4\left(\frac{\Delta t}{\hbar}H\right)^2.\end{aligned}$$

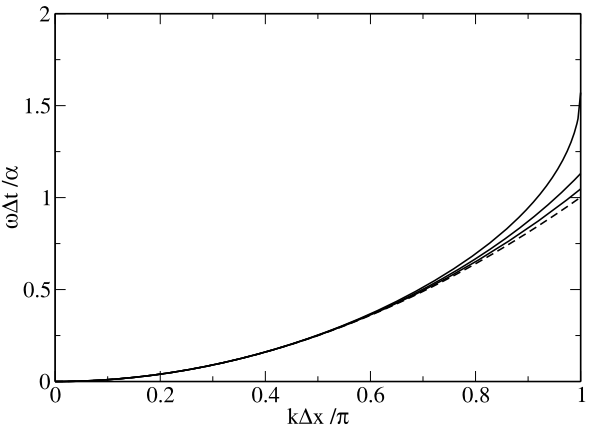

Fig. 21.4 (Dispersion of the Fourier method) The dispersion relation of the SOD-Fourier method (21.95) deviates from the exact dispersion (21.98) only for very high k-values and approaches it for small values of the stability parameter α. The scaled frequency $\omega\Delta t/\alpha$ is shown as a function of $k\Delta x/\pi$ for $\alpha = 0.5, 0.75, 1$ (*solid curves*) and compared with the exact relation of a free particle $\omega\Delta t/\alpha = (k\Delta x/\pi)^2$ (*dashed curve*)

Expanding the sine function we find the deviation from unitarity [10]

$$\mathcal{L}^\dagger\mathcal{L} - 1 = \frac{2}{3}\left(\frac{\Delta t}{\hbar}H\right)^4 + \cdots = O\left((\Delta t)^4\right) \tag{21.93}$$

which is of higher order than the error of the algorithm. Furthermore errors do not accumulate due to the stability of the algorithm (21.89). This also holds for deviations of the starting values from the condition (21.90).

The algorithm (21.84) can be combined with the finite differences method (Sect. 21.2.1.2)

$$\psi_m^{n+1} = \psi_m^{n-1} - 2\frac{\mathrm{i}\Delta t}{\hbar}\left[V_m\psi_m^n - \frac{\hbar^2}{2m_p\Delta x^2}\left(\psi_{m+1}^n + \psi_{m-1}^n - 2\psi_m^n\right)\right] \tag{21.94}$$

or with the pseudo-spectral Fourier method [150]. This combination needs two Fourier transformations for each step but it avoids the distortion of the dispersion relation inherent to the finite difference method. Inserting the plane wave (21.75) into (21.84) we find the dispersion relation (Fig. 21.4) for a free particle ($V = 0$):

$$\omega = \frac{1}{\Delta t}\arcsin\left(\frac{\hbar\Delta t k^2}{2m_p}\right) = \frac{1}{\Delta t}\arcsin\left(\alpha\left(\frac{k\Delta x}{\pi}\right)^2\right). \tag{21.95}$$

For a maximum k-value

$$k_{\max} = \frac{\pi}{\Delta x} \tag{21.96}$$

the stability condition (21.88) becomes

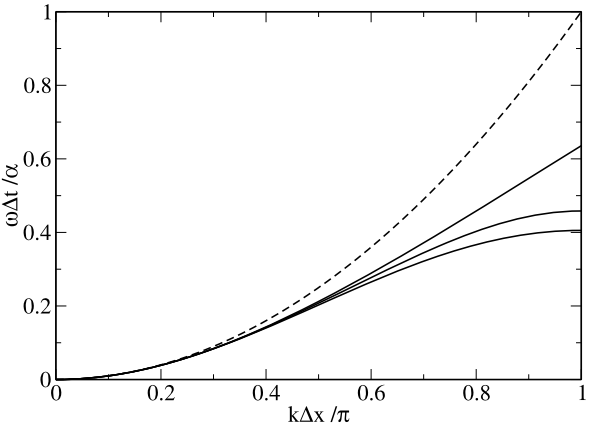

Fig. 21.5 (Dispersion of the finite difference method) The dispersion relation of the SOD-FD method (21.99) deviates largely from the exact dispersion (21.98), even for small values of the stability parameter α. The scaled frequency $\omega\Delta t/\alpha$ is shown as a function of $k\Delta x/\pi$ for $\alpha = \pi^2/4 \approx 2.467$, 1.85, 1.23, 0.2 (*solid curves*) and compared with the exact relation of a free particle $\omega\Delta t/\alpha = (k\Delta x/\pi)^2$ (*dashed curve*)

$$1 \geq \frac{\Delta t}{\hbar}\frac{\hbar^2 k_{\max}^2}{2m_p} = \alpha. \tag{21.97}$$

For small k the dispersion approximates the exact behavior

$$\omega = \frac{\hbar k^2}{2m_P}. \tag{21.98}$$

The finite difference method (21.94), on the other hand, has the dispersion relation (Fig. 21.5)

$$\omega = \frac{1}{\Delta t}\arcsin\left(\frac{4\alpha}{\pi^2}\sin^2\left(\frac{k\Delta x}{2}\right)\right) \tag{21.99}$$

and the stability limit

$$1 = \frac{\Delta t}{\hbar}E_{\max} = \frac{2\hbar\Delta t}{m_p\Delta x^2} = \frac{4\alpha}{\pi^2}. \tag{21.100}$$

The deviation from (21.98) is significant for $k\Delta x/\pi > 0.2$ even for small values of α [150].

21.2.2.3 Split-Operator Methods

The split-operator method approximates the exponential short time evolution operator as a product of exponential operators which are easier tractable. Starting from the Zassenhaus formula [164]

$$e^{\lambda(A+B)} = e^{\lambda A} e^{\lambda B} e^{\lambda^2 C_2} e^{\lambda^3 C_3} \dots \tag{21.101}$$

$$C_2 = \frac{1}{2}[B, A] \qquad C_3 = \frac{1}{6}[C_2, A + 2B] \quad \dots \tag{21.102}$$

approximants of increasing order can be systematically constructed [68, 246]

$$e^{\lambda(A+B)} = e^{\lambda A} e^{\lambda B} + O\left(\lambda^2\right) = e^{\lambda A} e^{\lambda B} e^{\lambda^2 C_2} + O\left(\lambda^3\right) \quad \dots . \tag{21.103}$$

Since these approximants do not conserve time reversibility, often the symmetric expressions

$$\begin{aligned} e^{\lambda(A+B)} &= e^{\lambda A/2} e^{\lambda B} e^{\lambda A/2} + O\left(\lambda^3\right) \\ &= e^{\lambda A/2} e^{\lambda B/2} e^{\lambda^2 C_3/4} e^{\lambda B/2} e^{\lambda A/2} + O\left(\lambda^5\right) \quad \dots \end{aligned} \tag{21.104}$$

are preferred.

Split-Operator-Fourier Method Dividing the Hamiltonian into its kinetic and potential parts

$$H = T + V = -\frac{\hbar^2}{2m_P} \frac{\partial^2}{\partial x^2} + V(x) \tag{21.105}$$

the time evolution operator can be approximated by the time-symmetric expression

$$U(\Delta t) = \mathrm{e}^{-\frac{\mathrm{i}\Delta t}{2\hbar} T} \mathrm{e}^{-\frac{\mathrm{i}\Delta t}{\hbar} V} \mathrm{e}^{-\frac{\mathrm{i}\Delta t}{2\hbar} T} + O\left((\Delta t)^3\right) \tag{21.106}$$

where the exponential of the kinetic energy can be easily applied in Fourier space [80, 150]. Combining several steps (21.106) to integrate over a longer time interval, consecutive operators can be combined to simplify the algorithm

$$U(N\Delta t) = U^N(\Delta t) = \mathrm{e}^{-\frac{\mathrm{i}\Delta t}{2\hbar} T} \left(\mathrm{e}^{-\frac{\mathrm{i}\Delta t}{\hbar} V} \mathrm{e}^{-\frac{\mathrm{i}\Delta t}{\hbar} T}\right)^{N-1} \mathrm{e}^{-\frac{\mathrm{i}\Delta t}{\hbar} V} \mathrm{e}^{-\frac{\mathrm{i}\Delta t}{2\hbar} T}. \tag{21.107}$$

Real-Space Product Formulae Using the discretization (21.48) on a regular grid the time evolution operator becomes the exponential of a matrix

$$\begin{aligned} &U(\Delta t) \\ &= \exp\left\{-\mathrm{i}\Delta t \begin{pmatrix} \frac{V_0}{\hbar} + \frac{\hbar}{m_P \Delta x^2} & -\frac{\hbar}{2m_P \Delta x^2} & & & \\ -\frac{\hbar}{2m_P \Delta x^2} & \frac{V_1}{\hbar} + \frac{\hbar}{m_P \Delta x^2} & -\frac{\hbar}{2m_P \Delta x^2} & & \\ & & \ddots & & \\ & & -\frac{\hbar}{2m_P \Delta x^2} & \frac{V_M}{\hbar} + \frac{\hbar}{m_P \Delta x^2} \end{pmatrix}\right\} \\ &= \exp\left\{-\mathrm{i}\Delta t \begin{pmatrix} \gamma_0 + 2\beta & -\beta & & \\ \beta & \gamma_1 + 2\beta & -\beta & \\ & & \ddots & \\ & & -\beta & \gamma_M + 2\beta \end{pmatrix}\right\} \end{aligned} \tag{21.108}$$

with the abbreviations

$$\gamma_m = \frac{1}{\hbar} V_m \quad \beta = \frac{\hbar}{2m_P \Delta x^2}. \tag{21.109}$$

The matrix can be decomposed into the sum of two overlapping tridiagonal block matrices [61, 67][5]

$$H_o = \begin{pmatrix} \gamma_0 + 2\beta & -\beta & & & \\ -\beta & \frac{1}{2}\gamma_1 + \beta & & & \\ & & \frac{1}{2}\gamma_2 + \beta & -\beta & \\ & & -\beta & \ddots & \end{pmatrix} = \begin{pmatrix} A_1 & & & \\ & A_3 & & \\ & & \ddots & \\ & & & A_{M-1} \end{pmatrix} \tag{21.110}$$

$$H_e = \begin{pmatrix} 0 & 0 & & & \\ 0 & \frac{1}{2}\gamma_1 + \beta & -\beta & & \\ & -\beta & \frac{1}{2}\gamma_2 + \beta & 0 & \\ & & 0 & \ddots & \end{pmatrix} = \begin{pmatrix} 0 & & & & \\ & A_2 & & & \\ & & \ddots & & \\ & & & A_{M-2} & \\ & & & & 0 \end{pmatrix} \tag{21.111}$$

The block structure simplifies the calculation of $e^{-\mathrm{i}\Delta t H_o}$ and $e^{-\mathrm{i}\Delta t H_e}$ tremendously since effectively only the exponential functions of 2×2 matrices

$$B_m(\tau) = e^{-\mathrm{i}\tau A_m} \tag{21.112}$$

have to be calculated and the approximation to the time evolution operator

$$\begin{aligned} U(\Delta t) &= e^{-\mathrm{i}\Delta t H_o/2} e^{-\mathrm{i}\Delta t H_e} e^{-\mathrm{i}\Delta t H_o/2} \\ &= \begin{pmatrix} B_1(\frac{\Delta t}{2}) & & \\ & B_3(\frac{\Delta t}{2}) & \\ & & \ddots \end{pmatrix} \begin{pmatrix} 1 & & \\ & B_2(\Delta t) & \\ & & \ddots \end{pmatrix} \\ &\quad \times \begin{pmatrix} B_1(\frac{\Delta t}{2}) & & \\ & B_3(\frac{\Delta t}{2}) & \\ & & \ddots \end{pmatrix} \end{aligned} \tag{21.113}$$

can be applied in real space without any Fourier transformation. To evaluate (21.112) the real symmetric matrix A_m is diagonalized by an orthogonal transformation (Sect. 9.2)

$$A = R^{-1} \tilde{A} R = R^{-1} \begin{pmatrix} \lambda_1 & 0 \\ 0 & \lambda_2 \end{pmatrix} R \tag{21.114}$$

and the exponential calculated from

$$e^{-\mathrm{i}\tau A} = 1 - \mathrm{i}\tau R^{-1} \tilde{A} R + \frac{(-\mathrm{i}\tau)^2}{2} R^{-1} \tilde{A} R \, R^{-1} \tilde{A} R + \cdots$$

[5] For simplicity only the case of even M is considered.

$$= R^{-1}\left[1 - \mathrm{i}\tau\tilde{A} + \frac{(-\mathrm{i}\tau)^2}{2}\tilde{A}R + \cdots\right]R$$
$$= R^{-1}e^{-\mathrm{i}\tau\tilde{A}}R = R^{-1}\begin{pmatrix} e^{-\mathrm{i}\tau\lambda_1} & \\ & e^{-\mathrm{i}\tau\lambda_2}\end{pmatrix}R. \tag{21.115}$$

21.2.3 Example: Free Wave Packet Motion

We simulate the free motion ($V = 0$) of a Gaussian wave packet along the x-axis (see Problem 21.1). To simplify the numerical calculation we set $\hbar = 1$ and $m_p = 1$ and solve the time dependent Schrödinger equation

$$\mathrm{i}\frac{\partial}{\partial t}\psi = -\frac{1}{2}\frac{\partial^2}{\partial x^2}\psi \tag{21.116}$$

for initial values given by a Gaussian wave packet with constant momentum

$$\psi_0(x) = \left(\frac{2}{a\pi}\right)^{1/4}\mathrm{e}^{\mathrm{i}k_0 x}\mathrm{e}^{-x^2/a}. \tag{21.117}$$

The exact solution can be easily found. Fourier transformation of (21.117) gives

$$\hat{\psi}_k(t=0) = \frac{1}{\sqrt{2\pi}}\int_{-\infty}^{\infty} dx\,\mathrm{e}^{-\mathrm{i}kx}\psi_0(x)$$
$$= \left(\frac{a}{2\pi}\right)^{1/4}\exp\left\{-\frac{a}{4}(k-k_0)^2\right\}. \tag{21.118}$$

Time evolution in k-space is rather simple

$$\mathrm{i}\frac{\partial}{\partial t}\hat{\psi}_k = \frac{k^2}{2}\hat{\psi}_k \tag{21.119}$$

hence

$$\hat{\psi}_k(t) = \mathrm{e}^{-\mathrm{i}k^2 t/2}\hat{\psi}_k(t=0) \tag{21.120}$$

and Fourier back transformation gives the solution of the time dependent Schrödinger equation in real space

$$\psi(t,x) = \frac{1}{\sqrt{2\pi}}\int_{-\infty}^{\infty} dx\,\mathrm{e}^{\mathrm{i}kx}\hat{\psi}_k(t)$$
$$= \left(\frac{2a}{\pi}\right)^{1/4}\frac{1}{\sqrt{a+2\mathrm{i}t}}\exp\left\{-\frac{(x-\mathrm{i}\frac{ak_0}{2})^2 + \frac{ak_0^2}{4}(a+2\mathrm{i}t)}{a+2\mathrm{i}t}\right\}. \tag{21.121}$$

Finally, the probability density is given by a Gaussian

$$\left|\psi(t,x)\right|^2 = \sqrt{\frac{2a}{\pi}}\frac{1}{\sqrt{a^2+4t^2}}\exp\left\{-\frac{2a}{a^2+4t^2}(x-k_0 t)^2\right\} \tag{21.122}$$

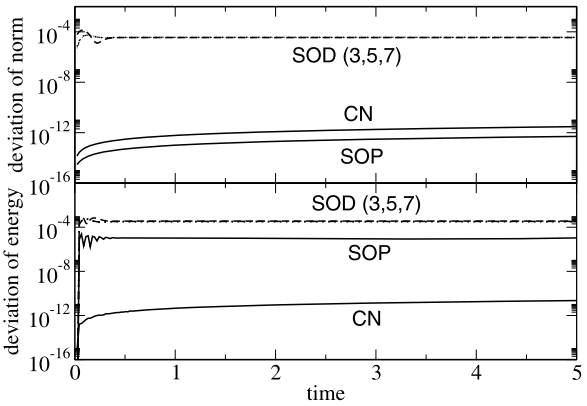

Fig. 21.6 (Conservation of norm and energy) The free motion of a Gaussian wave packet is simulated with the Crank-Nicolson method (CN) the second order differences method (SOD) with 3 point (21.48) 5 point (21.49) and 7-point (21.50) differences and with the real-space split-operator method (SPO). $\Delta t = 10^{-3}$, $\Delta x = 0.1$, $a = 1$, $k_0 = 3.77$

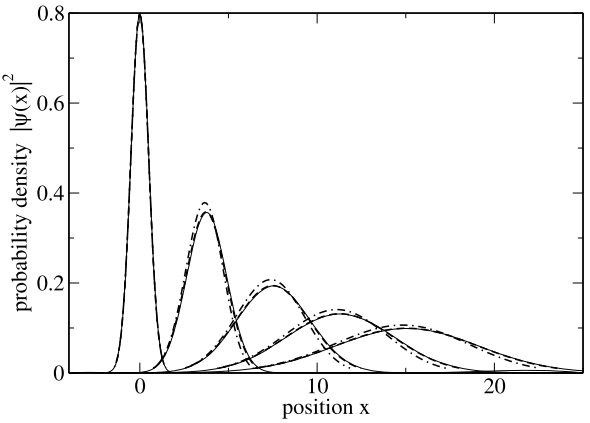

Fig. 21.7 (Free wave-packet motion) The free motion of a Gaussian wave packet is simulated. The probability density is shown for the initial Gaussian wave packet and at later times $t = 1, 2, 3, 4$. Results from the second order differences method with 3 point differences ((21.48), *dash-dotted*) and 5 point differences ((21.49), *dashed*) are compared with the exact solution ((21.122), *thin solid line*). $\Delta t = 10^{-3}$, $\Delta x = 0.1$, $a = 1$, $k_0 = 3.77$

which moves with constant velocity k_0 and kinetic energy

$$\int_{-\infty}^{\infty} dx\, \psi^*(x,t)\left(-\frac{\hbar^2}{2}\frac{\partial^2}{\partial x^2}\right)\psi(x,t) = \frac{1}{2}\left(k_0^2 + \frac{1}{a}\right). \tag{21.123}$$

Numerical results are shown in Figs. 21.6, 21.7 and Table 21.1.

21.3 Few-State Systems

In the following we discuss simple models which reduce the wavefunction to the superposition of a few important states, for instance an initial and a final state which are coupled by a resonant interaction. We approximate the solution of the time dependent Schrödinger equation as a linear combination

$$\big|\psi(t)\big\rangle \approx \sum_{j=1}^{M} C_j(t)|\phi_j\rangle \tag{21.124}$$

Table 21.1 (Accuracy of finite differences methods) The relative error of the kinetic energy (21.123) is shown as calculated with different finite difference methods

Method	E_{kin}	$\frac{E_{kin}-E_{kin}^{exact}}{E_{kin}^{exact}}$
Crank-Nicolson (CN) with 3 point differences	7.48608	-1.6×10^{-2}
Second Order Differences with 3 point differences (SOD3)	7.48646	-1.6×10^{-2}
Second Order Differences with 5 point differences (SOD5)	7.60296	-4.6×10^{-4}
Second Order Differences with 7 point differences (SOD7)	7.60638	-0.9×10^{-5}
Split-Operator method (SOP) with 3 point differences	7.48610	-1.6×10^{-2}
exact	7.60645	

of certain basis states $|\phi_1\rangle \cdots |\phi_M\rangle$[6] which are assumed to satisfy the necessary boundary conditions and to be orthonormalized

$$\langle \phi_i | \phi_j \rangle = \delta_{ij}. \tag{21.125}$$

Applying the method of weighted residuals (Sect. 11.4) we minimize the residual

$$|R\rangle = \mathrm{i}\hbar \sum_j \dot{C}_j(t)|\phi_j\rangle - \sum_j C_j(t) H |\phi_j\rangle \tag{21.126}$$

by choosing the basis functions as weight functions (Sect. 11.4.4) and solving the system of ordinary differential equations

$$0 = R_j = \langle \phi_j | R \rangle = \mathrm{i}\hbar \dot{C}_j - \sum_{j'} \langle \phi_j | H | \phi_{j'} \rangle C_{j'} \tag{21.127}$$

which can be written

$$\mathrm{i}\hbar \dot{C}_i = \sum_{j=1}^{M} H_{i,j} C_j(t) \tag{21.128}$$

with the matrix elements of the Hamiltonian

$$H_{i,j} = \langle \phi_i | H | \phi_j \rangle. \tag{21.129}$$

In matrix form (21.128) reads

$$\mathrm{i}\hbar \begin{pmatrix} \dot{C}_1(t) \\ \vdots \\ \dot{C}_M(t) \end{pmatrix} = \begin{pmatrix} H_{1,1} & \cdots & H_{1,M} \\ \vdots & \ddots & \vdots \\ H_{M,1} & \cdots & H_{M,M} \end{pmatrix} \begin{pmatrix} C_1(t) \\ \vdots \\ C_M(t) \end{pmatrix} \tag{21.130}$$

or more symbolically

$$\mathrm{i}\hbar \dot{\mathbf{C}}(t) = \mathbf{H}\mathbf{C}(t). \tag{21.131}$$

[6] This basis is usually incomplete.

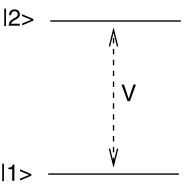

Fig. 21.8 Two-state system model

If the Hamilton operator does not depend explicitly on time ($H = \text{const.}$) the formal solution of (21.131) is given by

$$\mathbf{C} = \exp\left\{\frac{t}{i\hbar}H\right\}\mathbf{C}(0). \tag{21.132}$$

From the solution of the eigenvalue problem

$$H\mathbf{C}_\lambda = \lambda\mathbf{C}_\lambda \tag{21.133}$$

(eigenvalues λ and corresponding eigenvectors $\mathbf{C}_\lambda$) we build the linear combination

$$\mathbf{C} = \sum_\lambda a_\lambda \mathbf{C}_\lambda e^{\frac{\lambda}{i\hbar}t}. \tag{21.134}$$

The amplitudes a_λ can be calculated from the set of linear equations

$$\mathbf{C}(0) = \sum_\lambda a_\lambda \mathbf{C}_\lambda. \tag{21.135}$$

In the following we use the 4th order Runge-Kutta method to solve (21.131) numerically whereas the explicit solution (21.132) will be used to obtain approximate analytical results for special limiting cases.

A time dependent Hamiltonian $H(t)$ appears in semiclassical models which treat some of the slow degrees of freedom as classical quantities, for instance an electron in the Coulomb field of (slowly) moving nuclei

$$H(t) = T_{el} + \sum_j \frac{-q_j e}{4\pi\varepsilon_0|\mathbf{r} - \mathbf{R}_j(t)|} + \sum_{j<j'} \frac{q_j q_{j'}}{4\pi\varepsilon_0|\mathbf{R_j}(t) - \mathbf{R}_{j'}(t)|} \tag{21.136}$$

or in a time dependent electromagnetic field

$$H(t) = T_{el} + V_{el} - e\mathbf{r}\mathbf{E}(t). \tag{21.137}$$

21.3.1 Two-State System

The two-state system (also known as two-level system or TLS; Fig. 21.8) is the simplest model of interacting states and is very often used in physics, for instance in the context of quantum optics, quantum information, spintronics and quantum dots.

Its interaction matrix is

$$H = \begin{pmatrix} E_1 & V \\ V & E_2 \end{pmatrix} \tag{21.138}$$

and the equations of motion are

$$\begin{aligned} i\hbar\dot{C}_1 &= E_1 C_1 + V C_2 \\ i\hbar\dot{C}_2 &= E_2 C_2 + V C_1 . \end{aligned} \tag{21.139}$$

Equations (21.139) can be solved analytically but this involves some lengthy expressions. Let us therefore concentrate on two limiting cases:

(a) For $E_1 = E_2$ we add and subtract (21.139) to find

$$i\hbar \frac{\mathrm{d}}{\mathrm{d}t}(C_1 \pm C_2) = (E_1 \pm V)(C_1 \pm C_2) \tag{21.140}$$

with the solution

$$C_1 \pm C_2 = \big(C_1(0) \pm C_2(0)\big) e^{-it(E_1 \pm V)/\hbar} . \tag{21.141}$$

For initial conditions

$$C_1(0) = 1 \qquad C_2(0) = 0 \tag{21.142}$$

the explicit solution is given by

$$C_1 = e^{-itE_1/\hbar} \cos \frac{Vt}{\hbar} \qquad |C_1|^2 = \cos^2 \frac{Vt}{\hbar} = \frac{1 + \cos \frac{2Vt}{\hbar}}{2} \tag{21.143}$$

$$C_2 = -ie^{-itE_1/\hbar} \sin \frac{Vt}{\hbar} \qquad |C_2|^2 = \sin^2 \frac{Vt}{\hbar} = \frac{1 - \cos \frac{2Vt}{\hbar}}{2} \tag{21.144}$$

and the two-state system oscillates between the two states with the period

$$T = \frac{\pi\hbar}{V} . \tag{21.145}$$

(b) For $V \ll \Delta E = E_2 - E_1$[7] perturbation theory for the small quantity $V/\Delta E$ gives the following approximations:

$$\begin{aligned} \lambda_1 &\approx E_1 - \frac{V^2}{\Delta E} \\ \lambda_2 &\approx E_2 + \frac{V^2}{\Delta E} \end{aligned} \tag{21.146}$$

$$\begin{aligned} \mathbf{C}_1 &\approx \begin{pmatrix} 1 \\ \frac{V}{\Delta E} \end{pmatrix} \\ \mathbf{C}_2 &\approx \begin{pmatrix} \frac{-V}{\Delta E} \\ 1 \end{pmatrix} . \end{aligned} \tag{21.147}$$

For initial values $\mathbf{C}(0) = \binom{1}{0}$ the amplitudes $a_{1,2}$ are calculated from

$$\begin{pmatrix} 1 \\ 0 \end{pmatrix} = \begin{pmatrix} a_1 - a_2 \frac{V}{\Delta E} \\ a_1 \frac{V}{\Delta E} + a_2 \end{pmatrix} \tag{21.148}$$

[7] We assume $E_2 > E_1$.

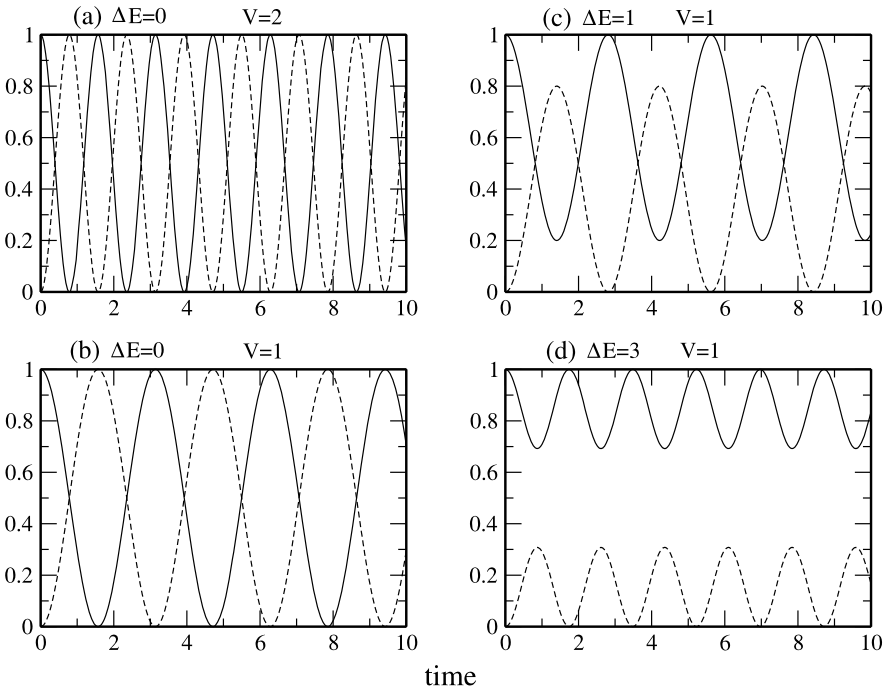

Fig. 21.9 (Numerical simulation of a two-state system) The equations of motion of the two-state system (21.139) are integrated with the 4th order Runge-Kutta method. For two resonant states the occupation probability of the initial state shows oscillations with the period (21.145) proportional to V^{-1}. With increasing energy gap $E_2 - E_1$ the amplitude of the oscillations decreases

which gives in lowest order

$$\begin{aligned} a_1 &\approx 1 - \frac{V^2}{\Delta E^2} \\ a_2 &\approx \frac{V^2}{\Delta E^2}. \end{aligned} \tag{21.149}$$

The approximate solution is

$$\mathbf{C} = \begin{pmatrix} (1 - \frac{V^2}{\Delta E^2}) e^{\frac{1}{i\hbar}(E_1 - \frac{V^2}{\Delta E^2})t} + \frac{V^2}{\Delta E^2} e^{\frac{1}{i\hbar}(E_2 + \frac{V^2}{\Delta E^2})t} \\ \frac{V}{\Delta E} e^{\frac{1}{i\hbar}(E_1 - \frac{V^2}{\Delta E^2})t} - \frac{V}{\Delta E} e^{\frac{1}{i\hbar}(E_2 + \frac{V^2}{\Delta E^2})t} \end{pmatrix} \tag{21.150}$$

and the occupation probability of the initial state is

$$|C_1|^2 \approx 1 - 2\frac{V^2}{\Delta E^2} + 2\frac{V^2}{\Delta E^2} \cos\left(\left(\Delta E + 2\frac{V^2}{\Delta E}\right)t\right). \tag{21.151}$$

Numerical results are shown in Fig. 21.9.

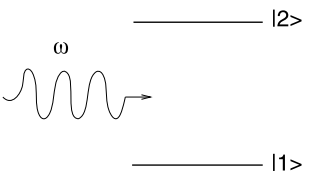

Fig. 21.10 Two-state system in an oscillating field

21.3.2 Two-State System with Time Dependent Perturbation

Consider now a 2-state system with an oscillating perturbation (for instance an atom or molecule in a laser field; Fig. 21.10)

$$H = \begin{pmatrix} E_1 & V(t) \\ V(t) & E_2 \end{pmatrix} \qquad V(t) = V_0 \cos \omega t. \tag{21.152}$$

The equations of motion are

$$\begin{aligned} \mathrm{i}\hbar \dot{C}_1 &= E_1 C_1 + V(t) C_2 \\ \mathrm{i}\hbar \dot{C}_2 &= V(t) C_1 + E_2 C_2. \end{aligned} \tag{21.153}$$

After the substitutions

$$\begin{aligned} C_1 &= \mathrm{e}^{\frac{E_1}{\mathrm{i}\hbar} t} u_1 \\ C_2 &= \mathrm{e}^{\frac{E_2}{\mathrm{i}\hbar} t} u_2 \end{aligned} \tag{21.154}$$

$$\omega_{21} = \frac{E_2 - E_1}{\hbar} \tag{21.155}$$

they become

$$\begin{aligned} \mathrm{i}\hbar \dot{u}_1 = V(t) \mathrm{e}^{\frac{E_2 - E_1}{\mathrm{i}\hbar} t} u_2 &= \frac{V_0}{2} \left(\mathrm{e}^{-\mathrm{i}(\omega_{21} - \omega)t} + \mathrm{e}^{-\mathrm{i}(\omega_{21} + \omega)t} \right) u_2 \\ \mathrm{i}\hbar \dot{u}_2 = V(t) e^{\frac{E_1 - E_2}{\mathrm{i}\hbar} t} u_1 &= \frac{V_0}{2} \left(\mathrm{e}^{\mathrm{i}(\omega_{21} - \omega)t} + \mathrm{e}^{\mathrm{i}(\omega_{21} + \omega)t} \right) u_1. \end{aligned} \tag{21.156}$$

At larger times the system oscillates between the two states.[8] Applying the rotating wave approximation for $\omega \approx \omega_{21}$ we neglect the fast oscillating perturbation

$$\mathrm{i}\hbar \dot{u}_1 = \frac{V_0}{2} \mathrm{e}^{-\mathrm{i}(\omega_{21} - \omega)t} u_2 \tag{21.157}$$

$$\mathrm{i}\hbar \dot{u}_2 = \frac{V_0}{2} \mathrm{e}^{\mathrm{i}(\omega_{21} - \omega)t} u_1 \tag{21.158}$$

and substitute

$$u_1 = a_1 \mathrm{e}^{-\mathrm{i}(\omega_{21} - \omega)t} \tag{21.159}$$

to have

[8] So called Rabi oscillations.

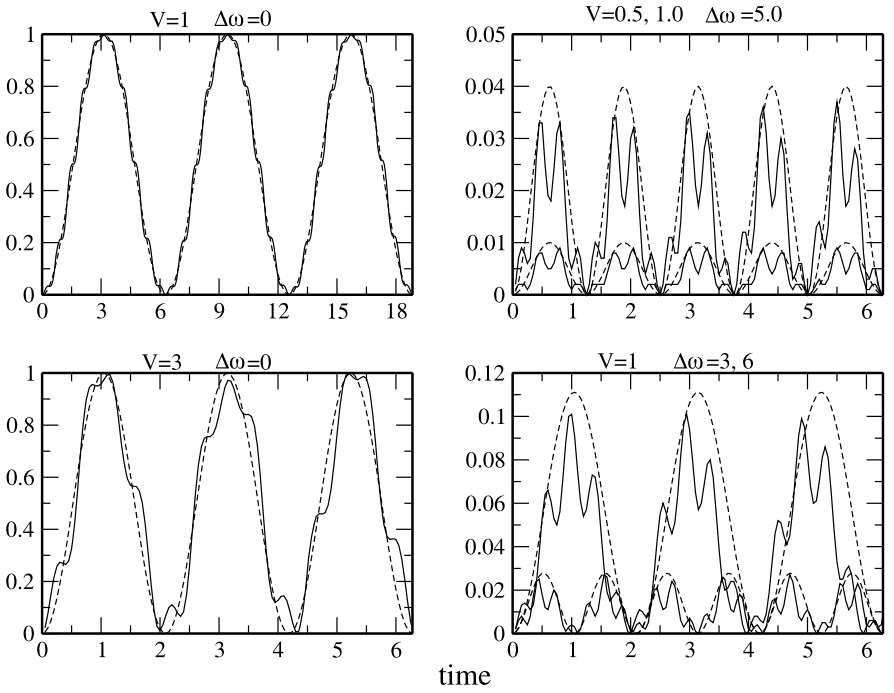

Fig. 21.11 (Simulation of a two-state system in an oscillating field) The equations of motion (21.153) are integrated with the 4th order Runge-Kutta method. At resonance the system oscillates between the two states with the frequency $V/\hbar$. The dashed curves show the corresponding solution of a two-state system with constant coupling (Sect. 21.3.1)

$$\mathrm{i}\hbar\big(\dot{a}_1 - a_1\mathrm{i}(\omega_{21}-\omega)\big)\mathrm{e}^{-\mathrm{i}(\omega_{21}-\omega)t} = \frac{V_0}{2}\mathrm{e}^{-\mathrm{i}(\omega_{21}-\omega)t}u_2 \tag{21.160}$$

$$\mathrm{i}\hbar\dot{u}_2 = \frac{V_0}{2}\mathrm{e}^{\mathrm{i}(\omega_{21}-\omega)t}\mathrm{e}^{-\mathrm{i}(\omega_{21}-\omega)t}a_1 \tag{21.161}$$

or

$$\mathrm{i}\hbar\dot{a}_1 = \hbar(\omega-\omega_{21})a_1 + \frac{V_0}{2}u_2 \tag{21.162}$$

$$\mathrm{i}\hbar\dot{u}_2 = \frac{V_0}{2}a_1 \tag{21.163}$$

which shows that the system behaves approximately like a two-state system with a constant interaction $V_0/2$ and an energy gap $\hbar(\omega_{21}-\omega) = E_2 - E_1 - \hbar\omega$ (a comparison with a full numerical calculation is shown in Fig. 21.11).

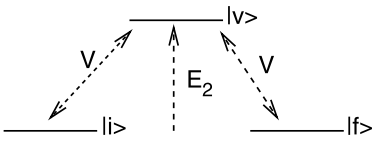

Fig. 21.12 Superexchange model

21.3.3 Superexchange Model

The concept of superexchange was originally formulated for magnetic interactions [8] and later introduced to electron transfer theory [117]. It describes an indirect interaction through high energy intermediates (Fig. 21.12). In the simplest case, we have to consider two isoenergetic states i and f which do not interact directly but via coupling to an intermediate state v.

The interaction matrix is

$$H = \begin{pmatrix} 0 & V_1 & 0 \\ V_1 & E_2 & V_2 \\ 0 & V_2 & 0 \end{pmatrix}. \tag{21.164}$$

For simplification we choose $V_1 = V_2$.

Let us first consider the special case of a resonant intermediate state $E_2 = 0$:

$$H = \begin{pmatrix} 0 & V & 0 \\ V & 0 & V \\ 0 & V & 0 \end{pmatrix}. \tag{21.165}$$

Obviously one eigenvalue is $\lambda_1 = 0$ and the corresponding eigenvector is

$$\mathbf{C}_1 = \begin{pmatrix} 1 \\ 0 \\ -1 \end{pmatrix}. \tag{21.166}$$

The two remaining eigenvalues are solutions of

$$0 = \det \begin{vmatrix} -\lambda & V & 0 \\ V & -\lambda & V \\ 0 & V & -\lambda \end{vmatrix} = \lambda\left(-\lambda^2 + 2V^2\right) \tag{21.167}$$

which gives

$$\lambda_{2,3} = \pm\sqrt{2}V. \tag{21.168}$$

The eigenvectors are

$$\mathbf{C}_{2,3} = \begin{pmatrix} 1 \\ \pm\sqrt{2} \\ 1 \end{pmatrix}. \tag{21.169}$$

From the initial values

$$\mathbf{C}(0) = \begin{pmatrix} a_1 + a_2 + a_3 \\ \sqrt{2}a_2 - \sqrt{2}a_3 \\ -a_1 + a_2 + a_3 \end{pmatrix} = \begin{pmatrix} 1 \\ 0 \\ 0 \end{pmatrix} \tag{21.170}$$

the amplitudes are calculated as

$$a_1 = \frac{1}{2}\, a_2 = a_3 = \frac{1}{4} \tag{21.171}$$

and finally the solution is

$$\begin{aligned}\mathbf{C} &= \frac{1}{2}\begin{pmatrix}1\\0\\-1\end{pmatrix} + \frac{1}{4}\begin{pmatrix}1\\\sqrt{2}\\1\end{pmatrix} e^{\frac{1}{i\hbar}\sqrt{2}Vt} + \frac{1}{4}\begin{pmatrix}1\\-\sqrt{2}\\1\end{pmatrix} e^{-\frac{1}{i\hbar}\sqrt{2}Vt} \\ &= \begin{pmatrix}\frac{1}{2} + \frac{1}{2}\cos\frac{\sqrt{2}V}{\hbar}t\\ \frac{\sqrt{2}}{2} i \sin\frac{\sqrt{2}V}{\hbar}t\\ -\frac{1}{2} + \frac{1}{2}\cos\frac{\sqrt{2}V}{\hbar}t\end{pmatrix}.\end{aligned} \tag{21.172}$$

Let us now consider the case of a distant intermediate state $V \ll |E_2|$. $\lambda_1 = 0$ and the corresponding eigenvector still provide one solution. The two other eigenvalues are approximately given by

$$\lambda_{2,3} = \pm\sqrt{\frac{E_2^2}{4} + 2V^2} + \frac{E_2}{2} \approx \frac{E_2}{2} \pm \frac{E_2}{2}\left(1 + \frac{4V^2}{E_2^2}\right) \tag{21.173}$$

$$\lambda_2 \approx E_2 + \frac{2V^2}{E_2} \qquad \lambda_3 \approx -\frac{2V^2}{E_2} \tag{21.174}$$

and the eigenvectors by

$$\mathbf{C}_2 \approx \begin{pmatrix}1\\\frac{E_2}{V} + \frac{2V}{E_2}\\1\end{pmatrix} \qquad \mathbf{C}_3 \approx \begin{pmatrix}1\\-\frac{2V}{E_2}\\1\end{pmatrix}. \tag{21.175}$$

From the initial values

$$\mathbf{C}(0) = \begin{pmatrix}1\\0\\0\end{pmatrix} = \begin{pmatrix}a_1 + a_2 + a_3\\ a_2\lambda_2 + a_3\lambda_3\\ -a_1 + a_2 + a_3\end{pmatrix} \tag{21.176}$$

we calculate the amplitudes

$$a_1 = \frac{1}{2} \qquad a_2 \approx \frac{V^2}{E_2^2} \qquad a_3 \approx \frac{1}{2}\left(1 - \frac{2V^2}{E_2^2}\right) \tag{21.177}$$

and finally the solution

$$\mathbf{C} \approx \begin{pmatrix}\frac{1}{2}(1 + e^{-\frac{1}{i\hbar}\frac{2V^2}{E_2}t})\\ \frac{V}{E_2} e^{\frac{1}{i\hbar}E_2 t} - \frac{2V}{E_2} e^{-\frac{1}{i\hbar}\frac{2V^2}{E_2}t}\\ \frac{1}{2}(-1 + e^{-\frac{1}{i\hbar}\frac{2V^2}{E_2}t})\end{pmatrix}. \tag{21.178}$$

The occupation probability of the initial state is

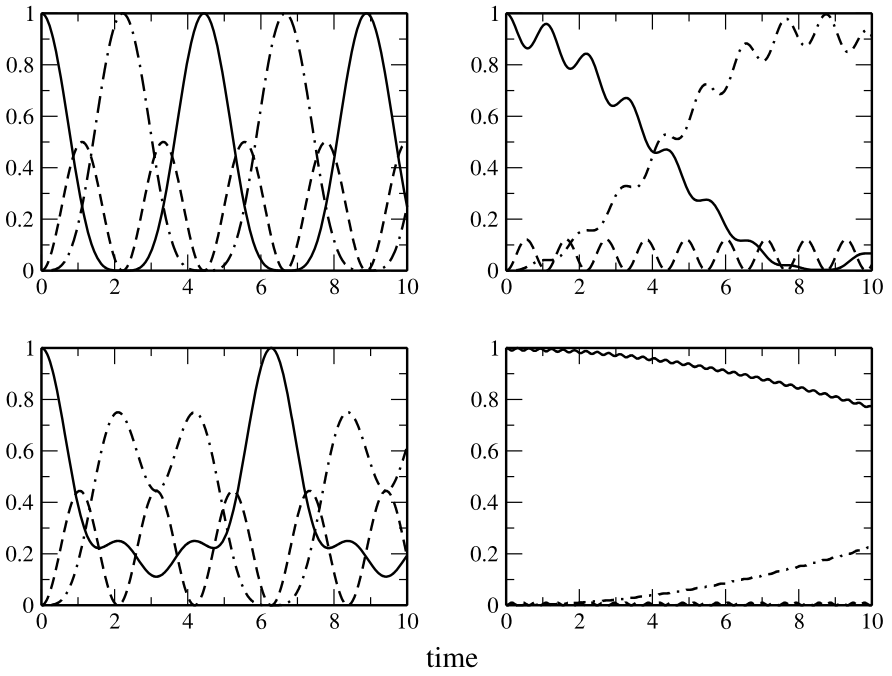

Fig. 21.13 (Numerical simulation of the superexchange model) The equations of motion for the model (21.164) are solved numerically with the 4th order Runge-Kutta method. The energy gap is varied to study the transition from the simple oscillation with $\omega = \sqrt{2}V/\hbar$ (21.172) to the effective two-state system with $\omega = V_{eff}/\hbar$ (21.179). Parameters are $V_1 = V_2 = 1$, $E_1 = E_3 = 0$, $E_2 = 0, 1, 5, 20$. The occupation probability of the initial (*solid curves*), virtual intermediate (*dashed curves*) and final (*dash-dotted curves*) state are shown

$$|C_1|^2 = \frac{1}{4}\left|1 + e^{-\frac{1}{i\hbar}\frac{2V^2}{E_2}t}\right|^2 = \cos^2\left(\frac{V^2}{\hbar E_2}t\right) \tag{21.179}$$

which shows that the system behaves like a 2-state system with an effective interaction of

$$V_{eff} = \frac{V^2}{E_2}. \tag{21.180}$$

Numerical results are shown in Fig. 21.13.

21.3.4 Ladder Model for Exponential Decay

For time independent Hamiltonian the solution (21.132) of the Schrödinger equation is a sum of oscillating terms and the quantum recurrence theorem [29] states that the system returns to the initial state arbitrarily closely after a certain time T_r. However, if the initial state is coupled to a larger number of final states, the recurrence time can become very long and an exponential decay observed over a large period. The ladder

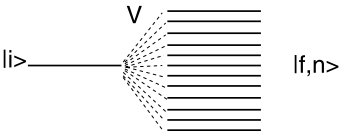

Fig. 21.14 Ladder model

model [27, 242] considers an initial state $|0\rangle$ interacting with a manifold of states $|1\rangle \cdots |n\rangle$, which do not interact with each other and are equally spaced (Fig. 21.14)

$$H = \begin{pmatrix} 0 & V & \cdots & V \\ V & E_1 & & \\ \vdots & & \ddots & \\ V & & & E_n \end{pmatrix} \qquad E_j = E_1 + (j-1)\Delta E. \tag{21.181}$$

The equations of motion are

$$\begin{aligned} \mathrm{i}\hbar \dot{C}_0 &= V \sum_{j=1}^{n} C_j \\ \mathrm{i}\hbar \dot{C}_j &= E_j C_j + V C_0. \end{aligned} \tag{21.182}$$

For the special case $\Delta E = 0$ we simply have

$$\ddot{C}_0 = -\frac{V^2}{\hbar^2} n C_0 \tag{21.183}$$

with an oscillating solution

$$C_0 \sim \cos\left(\frac{V\sqrt{n}}{\hbar} t\right). \tag{21.184}$$

Here the n states act like one state with an effective coupling of $V\sqrt{n}$.

For the general case $\Delta E \neq 0$ we substitute

$$C_j = u_j \mathrm{e}^{\frac{E_j}{\mathrm{i}\hbar} t} \tag{21.185}$$

and have

$$\mathrm{i}\hbar \dot{u}_j \mathrm{e}^{\frac{E_j}{\mathrm{i}\hbar} t} = V C_0. \tag{21.186}$$

Integration gives

$$u_j = \frac{V}{\mathrm{i}\hbar} \int_{t_0}^{t} \mathrm{e}^{-\frac{E_j}{\mathrm{i}\hbar} t'} C_0\big(t'\big)\, dt' \tag{21.187}$$

and therefore

$$C_j = \frac{V}{\mathrm{i}\hbar} \int_{t_0}^{t} \mathrm{e}^{\mathrm{i}\frac{E_j}{\hbar}(t'-t)} C_0\big(t'\big)\, dt'. \tag{21.188}$$

With the definition

$$E_j = j * \hbar \Delta\omega \tag{21.189}$$

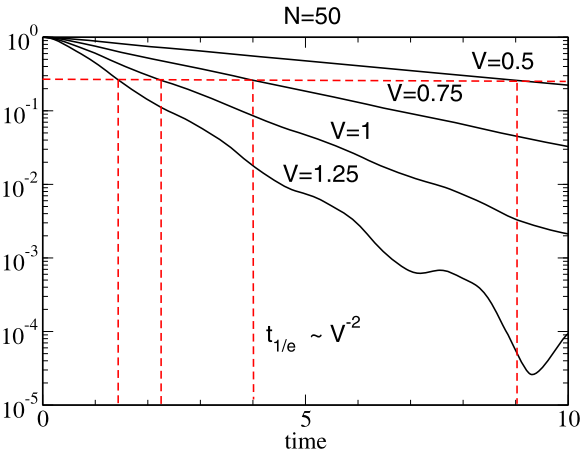

Fig. 21.15 (Numerical solution of the ladder model) The time evolution of the ladder model (21.182) is calculated with the 4th order Runge-Kutta method for $N = 50$ states and different values of the coupling V

we have

$$\dot{C}_0 = \frac{V}{\mathrm{i}\hbar} \sum_{j=1}^{n} C_j = -\frac{V^2}{\hbar^2} \sum_j \int_{t_0}^{t} \mathrm{e}^{\mathrm{i}j\Delta\omega(t'-t)} C_0(t')\, dt'. \tag{21.190}$$

We replace the sum by an integral over the continuous variable

$$\omega = j\Delta\omega \tag{21.191}$$

and extend the integration range to $-\infty \cdots \infty$. Then the sum becomes approximately a delta function

$$\sum_{j=-\infty}^{\infty} \mathrm{e}^{\mathrm{i}j\Delta\omega(t'-t)} \Delta j \;\to\; \int_{-\infty}^{\infty} \mathrm{e}^{\mathrm{i}\omega(t'-t)} \frac{d\omega}{\Delta\omega} = \frac{2\pi}{\Delta\omega} \delta(t-t') \tag{21.192}$$

and the final result is an exponential decay law

$$\dot{C}_0 = -\frac{2\pi V^2}{\hbar^2 \Delta\omega} C_0 = -\frac{2\pi V^2}{\hbar} \rho(E) C_0 \tag{21.193}$$

with the density of final states

$$\rho(E) = \frac{1}{\hbar\Delta\omega} = \frac{1}{\Delta E}. \tag{21.194}$$

Numerical results are shown in Fig. 21.15.

21.3.5 Landau-Zener Model

This model describes crossing of two states (Fig. 21.16), for instance for colliding atoms or molecules [154, 282]. It is assumed that the interaction V is constant near the crossing point and that the nuclei move classically with constant velocity

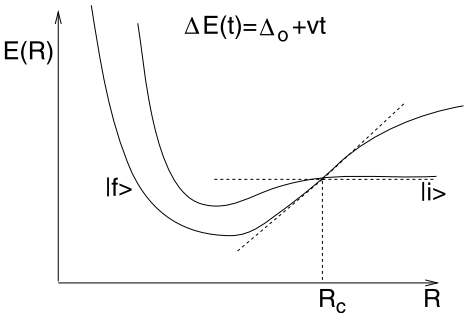

Fig. 21.16 Slow atomic collision

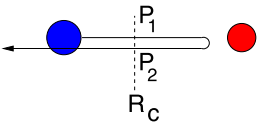

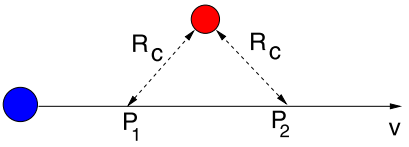

$P_{Tr} = P_1(1-P_2) + (1-P_1)P_2 = 2P(1-P)$

Fig. 21.17 Multiple passage of the interaction region

$$H = \begin{pmatrix} 0 & V \\ V & \Delta E(t) \end{pmatrix} \qquad \Delta E(t) = \Delta E_0 + vt. \tag{21.195}$$

For small interaction V or large velocity $\frac{\partial}{\partial t}\Delta E = \dot{Q}\frac{\partial}{\partial Q}\Delta E$ the transition probability can be calculated with perturbation theory to give

$$P = \frac{2\pi V^2}{\hbar \frac{\partial}{\partial t}\Delta E}. \tag{21.196}$$

This expression becomes invalid for small velocities. Here the system stays on the adiabatic potential surface, i.e. $P \to 1$. Landau and Zener found the following expression which is valid in both limits:

$$P_{LZ} = 1 - \exp\left(-\frac{2\pi V^2}{\hbar \frac{\partial}{\partial t}\Delta E}\right). \tag{21.197}$$

In case of collisions multiple crossing of the interaction region has to be taken into account (Fig. 21.17). Numerical results are shown in Fig. 21.18.

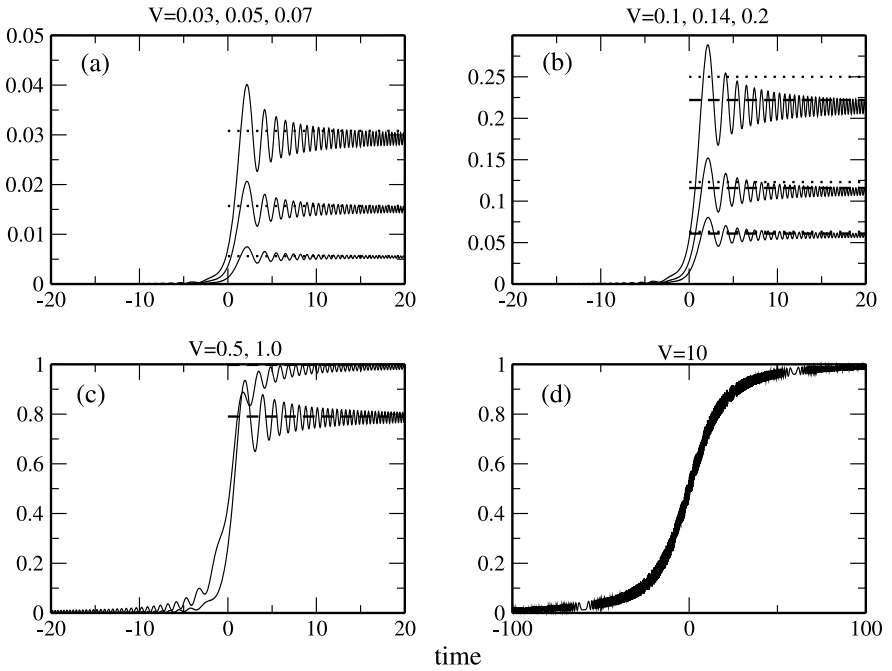

Fig. 21.18 (Numerical solution of the Landau-Zener model) Numerical calculations (*solid curves*) are compared with the Landau-Zener probability ((21.197), *dashed lines*) and the approximation ((21.196), *dotted lines*). The velocity is $\mathrm{d}\Delta E/\mathrm{d}t = 1$

21.4 The Dissipative Two-State System

A two-state quantum system coupled to a thermal bath serves as a model for magnetic resonance phenomena, coherent optical excitations [263, 280] and, quite recently, for a qubit, the basic element of a future quantum computer [73, 183]. Its quantum state can not be described by a single wavefunction. Instead mixed quantum states have to be considered which can be conveniently described within the density matrix formalism [232].

21.4.1 Equations of Motion for a Two-State System

The equations of motion for a two-state system are

$$i\hbar\dot{\rho}_{11} = H_{12}\rho_{21} - \rho_{12}H_{21} \tag{21.198}$$

$$i\hbar\dot{\rho}_{22} = H_{21}\rho_{12} - \rho_{21}H_{12} \tag{21.199}$$

$$i\hbar\dot{\rho}_{12} = (H_{11} - H_{22})\rho_{12} + H_{12}(\rho_{22} - \rho_{11}) \tag{21.200}$$

$$-i\hbar\dot{\rho}_{21} = (H_{11} - H_{22})\rho_{21} + H_{21}(\rho_{22} - \rho_{11}) \tag{21.201}$$

which can be arranged as a system of linear equations[9]

$$i\hbar \begin{pmatrix} \dot{\rho}_{11} \\ \dot{\rho}_{22} \\ \dot{\rho}_{12} \\ \dot{\rho}_{21} \end{pmatrix} = \begin{pmatrix} 0 & 0 & -H_{21} & H_{12} \\ 0 & 0 & H_{21} & -H_{12} \\ -H_{12} & H_{12} & H_{11} - H_{22} & 0 \\ H_{21} & -H_{21} & 0 & H_{22} - H_{11} \end{pmatrix} \begin{pmatrix} \rho_{11} \\ \rho_{22} \\ \rho_{12} \\ \rho_{21} \end{pmatrix}. \tag{21.202}$$

21.4.2 The Vector Model

The density matrix is Hermitian

$$\rho_{ij} = \rho_{ji}^* \tag{21.203}$$

its diagonal elements are real valued and due to conservation of probability

$$\rho_{11} + \rho_{22} = \text{const.} \tag{21.204}$$

Therefore the four elements of the density matrix can be specified by three real parameters, which are usually chosen as

$$x = 2\Re\rho_{21} \tag{21.205}$$

$$y = 2\Im\rho_{21} \tag{21.206}$$

$$z = \rho_{11} - \rho_{22} \tag{21.207}$$

and satisfy the equations

$$\frac{\mathrm{d}}{\mathrm{d}t} 2\Re(\rho_{21}) = -\frac{1}{\hbar}\big((H_{11} - H_{22})2\Im(\rho_{21}) + 2\Im(H_{12})(\rho_{11} - \rho_{22})\big) \tag{21.208}$$

$$\frac{\mathrm{d}}{\mathrm{d}t} 2\Im(\rho_{21}) = \frac{1}{\hbar}\big((H_{11} - H_{22})2\Re(\rho_{21}) - 2\Re(H_{12})(\rho_{11} - \rho_{22})\big) \tag{21.209}$$

$$\frac{\mathrm{d}}{\mathrm{d}t}(\rho_{11} - \rho_{22}) = \frac{2}{\hbar}\big(\Im(H_{12})2\Re(\rho_{21}) + \Re H_{12} 2\Im(\rho_{21})\big). \tag{21.210}$$

Together they form the Bloch vector

$$\mathbf{r} = \begin{pmatrix} x \\ y \\ z \end{pmatrix} \tag{21.211}$$

which is often used to visualize the time evolution of a two-state system [81]. In terms of the Bloch vector the density matrix is given by

$$\begin{pmatrix} \rho_{11} & \rho_{12} \\ \rho_{21} & \rho_{22} \end{pmatrix} = \begin{pmatrix} \frac{1+z}{2} & \frac{x-iy}{2} \\ \frac{x+iy}{2} & \frac{1-z}{2} \end{pmatrix} = \frac{1}{2}(1 + \mathbf{r}\boldsymbol{\sigma}) \tag{21.212}$$

[9] The matrix of this system corresponds to the Liouville operator.

with the Pauli matrices

$$\sigma_x = \begin{pmatrix} 0 & 1 \\ 1 & 0 \end{pmatrix}, \qquad \sigma_y = \begin{pmatrix} 0 & -\mathrm{i} \\ \mathrm{i} & 0 \end{pmatrix}, \qquad \sigma_z = \begin{pmatrix} 1 & \\ & -1 \end{pmatrix}. \tag{21.213}$$

From (21.208), (21.209), (21.210) we obtain the equation of motion

$$\frac{\mathrm{d}}{\mathrm{d}t}\begin{pmatrix} x \\ y \\ z \end{pmatrix} = \begin{pmatrix} -y\,\frac{H_{11}-H_{22}}{\hbar} - z\,\frac{2\Im(H_{12})}{\hbar} \\ x\,\frac{H_{11}-H_{22}}{\hbar} - z\,\frac{2\Re(H_{12})}{\hbar} \\ x\,\frac{2\Im(H_{12})}{\hbar} + y\,\frac{2\Re(H_{12})}{\hbar} \end{pmatrix} \tag{21.214}$$

which can be written as a cross product

$$\frac{\mathrm{d}}{\mathrm{d}t}\mathbf{r} = \boldsymbol{\omega} \times \mathbf{r} \tag{21.215}$$

with

$$\boldsymbol{\omega} = \begin{pmatrix} \frac{2}{\hbar}\Re H_{12} \\ -\frac{2}{\hbar}\Im H_{12} \\ \frac{1}{\hbar}(H_{11} - H_{22}) \end{pmatrix}. \tag{21.216}$$

Any normalized pure quantum state of the two-state system can be written as [75]

$$|\psi\rangle = \begin{pmatrix} C_1 \\ C_2 \end{pmatrix} = \cos\frac{\theta}{2}\begin{pmatrix} 1 \\ 0 \end{pmatrix} + \mathrm{e}^{\mathrm{i}\phi}\sin\frac{\theta}{2}\begin{pmatrix} 0 \\ 1 \end{pmatrix} \tag{21.217}$$

corresponding to the density matrix

$$\rho = \begin{pmatrix} \cos^2\frac{\theta}{2} & \mathrm{e}^{-\mathrm{i}\phi}\sin\frac{\theta}{2}\cos\frac{\theta}{2} \\ \mathrm{e}^{\mathrm{i}\phi}\sin\frac{\theta}{2}\cos\frac{\theta}{2} & \sin^2\frac{\theta}{2} \end{pmatrix}. \tag{21.218}$$

The Bloch vector

$$\mathbf{r} = \begin{pmatrix} \cos\phi\sin\theta \\ \sin\phi\sin\theta \\ \cos\theta \end{pmatrix} \tag{21.219}$$

represents a point on the unit sphere (the Bloch sphere, Fig. 21.19). Mixed states correspond to the interior of the Bloch sphere with the fully mixed state $\rho = \left(\begin{smallmatrix} 1/2 & 0 \\ 0 & 1/2 \end{smallmatrix}\right)$ represented by the center of the sphere (Fig. 21.19).

21.4.3 The Spin-$\frac{1}{2}$ System

An important example of a two-state system is a particle with spin $\frac{1}{2}$. Its quantum state can be described by a two-component vector

$$\begin{pmatrix} C_1 \\ C_2 \end{pmatrix} = C_1\begin{pmatrix} 1 \\ 0 \end{pmatrix} + C_2\begin{pmatrix} 0 \\ 1 \end{pmatrix} \tag{21.220}$$

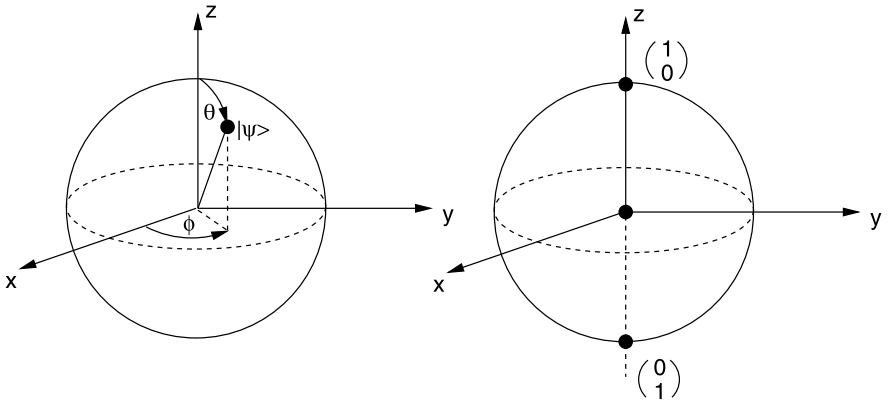

Fig. 21.19 (Bloch sphere) *Left*: Any pure quantum state of a two-state system can be represented by a point on the Bloch sphere. *Right*: The poles represent the basis states. Mixed quantum states correspond to the interior of the sphere, the center represents the fully mixed state

where the two unit vectors are eigenvectors of the spin component in z-direction corresponding to the eigenvalues $s_z = \pm\frac{\hbar}{2}$. The components of the spin operator are given by the Pauli matrices

$$S_i = \frac{\hbar}{2}\sigma_i \tag{21.221}$$

and have expectation values

$$\langle \mathbf{S} \rangle = \frac{\hbar}{2}\begin{pmatrix} C_1^* & C_2^* \end{pmatrix}\begin{pmatrix} \sigma_x \\ \sigma_y \\ \sigma_z \end{pmatrix}\begin{pmatrix} C_1 \\ C_2 \end{pmatrix} = \hbar\begin{pmatrix} \frac{C_1^* C_2 + C_2^* C_1}{2} \\ \frac{C_1^* C_2 - C_2^* C_1}{2i} \\ \frac{|C_1|^2 - |C_2|^2}{2} \end{pmatrix}. \tag{21.222}$$

The ensemble average for a system of spin-$\frac{1}{2}$ particles is given by the Bloch vector

$$\overline{\langle \mathbf{S} \rangle} = \hbar\begin{pmatrix} \frac{\rho_{21} + \rho_{12}}{2} \\ \frac{\rho_{21} - \rho_{12}}{2\mathrm{i}} \\ \frac{\rho_{11} - \rho_{22}}{2} \end{pmatrix} = \frac{\hbar}{2}\mathbf{r}. \tag{21.223}$$

The Hamiltonian of a spin-$\frac{1}{2}$ particle in a magnetic field $\mathbf{B}$ is

$$H = -\gamma\frac{\hbar}{2}\boldsymbol{\sigma}\mathbf{B} = -\gamma\frac{\hbar}{2}\begin{pmatrix} B_z & B_x - \mathrm{i}B_y \\ B_x + \mathrm{i}B_y & -B_z \end{pmatrix} \tag{21.224}$$

from which the following relations are obtained

$$\gamma B_x = -\frac{2}{\hbar}\Re H_{12} \tag{21.225}$$

$$\gamma B_y = \frac{2}{\hbar}\Im H_{12} \tag{21.226}$$

$$\gamma B_z = -\frac{H_{11} - H_{22}}{\hbar} \tag{21.227}$$

$$\boldsymbol{\omega} = -\gamma \mathbf{B}. \tag{21.228}$$

The average magnetization

$$\mathbf{m} = \gamma \overline{\langle \mathbf{S} \rangle} = \gamma \frac{\hbar}{2} \mathbf{r} \tag{21.229}$$

obeys the equation of motion

$$\frac{\mathrm{d}}{\mathrm{d}t} \mathbf{m} = -\gamma \mathbf{B} \times \mathbf{m}. \tag{21.230}$$

21.4.4 Relaxation Processes—The Bloch Equations

Relaxation of the nuclear magnetization due to interaction with the environment was first described phenomenologically by Bloch in 1946 [28]. A more rigorous description was given later [201, 269] and also applied to optical transitions [179]. Recently electron spin relaxation has attracted much interest in the new field of spintronics [284] and the dissipative two-state system has been used to describe the decoherence of a qubit [46].

21.4.4.1 Phenomenological Description

In thermal equilibrium the density matrix is given by a canonical distribution

$$\rho^{eq} = \frac{\mathrm{e}^{-\beta H}}{\mathrm{tr}(\mathrm{e}^{-\beta H})} \tag{21.231}$$

which for a two-state system without perturbation

$$H_0 = \begin{pmatrix} \frac{\Delta}{2} & \\ & -\frac{\Delta}{2} \end{pmatrix} \tag{21.232}$$

becomes

$$\rho^{eq} = \begin{pmatrix} \frac{\mathrm{e}^{-\beta\Delta/2}}{\mathrm{e}^{\beta\Delta/2}+\mathrm{e}^{-\beta\Delta/2}} & \\ & \frac{\mathrm{e}^{\beta\Delta/2}}{\mathrm{e}^{\beta\Delta/2}+\mathrm{e}^{-\beta\Delta/2}} \end{pmatrix} \tag{21.233}$$

where, as usually $\beta = 1/k_B T$. If the energy gap is very large $\Delta \gg k_B T$ like for an optical excitation, the equilibrium state is the state with lower energy[10]

$$\rho^{eq} = \begin{pmatrix} 0 & 0 \\ 0 & 1 \end{pmatrix}. \tag{21.234}$$

[10]We assume $\Delta \geq 0$, such that the equilibrium value of $z = \rho_{11} - \rho_{22}$ is negative. Eventually, the two states have to be exchanged.

The phenomenological model assumes that deviations of the occupation difference from its equilibrium value

$$\rho_{11}^{eq} - \rho_{22}^{eq} = -\tanh\left(\frac{\Delta}{2k_B T}\right) \tag{21.235}$$

decay exponentially with a time constant T_1 (for NMR this is the spin-lattice relaxation time)

$$\frac{d}{dt}_{|Rel}(\rho_{11} - \rho_{22}) = -\frac{1}{T_1}\left[(\rho_{11} - \rho_{22}) - \left(\rho_{11}^{eq} - \rho_{22}^{eq}\right)\right]. \tag{21.236}$$

The coherence of the two states decays exponentially with a time constant T_2 which is closely related to T_1 in certain cases[11] but can be much smaller than T_1 if there are additional dephasing mechanisms. The equation

$$\frac{d}{dt}_{|Rel}\rho_{12} = -\frac{1}{T_2}\rho_{12} \tag{21.237}$$

describes the decay of the transversal polarization due to spatial and temporal differences of different spins (spin-spin relaxation), whereas for an optical excitation or a qubit it describes the loss of coherence of a single two-state system due to interaction with its environment.

The combination of (21.230) and the relaxation terms (21.236), (21.237) gives the Bloch equations [28] which were originally formulated to describe the time evolution of the macroscopic polarization

$$\frac{\mathrm{d}\mathbf{m}}{\mathrm{d}t} = -\gamma\mathbf{B}\times\mathbf{m} - R(\mathbf{m} - \mathbf{m}_{eq}) \qquad R = \begin{pmatrix} \frac{1}{T_2} & 0 & 0 \\ 0 & \frac{1}{T_2} & 0 \\ 0 & 0 & \frac{1}{T_1} \end{pmatrix}. \tag{21.238}$$

For the components of the Bloch vector they read explicitly

$$\frac{\mathrm{d}}{\mathrm{d}t}\begin{pmatrix} x \\ y \\ z \end{pmatrix} = \begin{pmatrix} -1/T_2 & -\frac{1}{\hbar}(H_{11} - H_{22}) & -\frac{2}{\hbar}\Im H_{12} \\ \frac{1}{\hbar}(H_{11} - H_{22}) & -1/T_2 & -\frac{2}{\hbar}\Re H_{12} \\ \frac{2}{\hbar}\Im H_{12} & \frac{2}{\hbar}\Re H_{12} & -1/T_1 \end{pmatrix}\begin{pmatrix} x \\ y \\ z \end{pmatrix} + \begin{pmatrix} 0 \\ 0 \\ z_{eq}/T_1 \end{pmatrix}. \tag{21.239}$$

21.4.5 The Driven Two-State System

The Hamiltonian of a two-state system (for instance an atom or molecule) in an oscillating electric field $E\mathrm{e}^{-\mathrm{i}\omega_f t}$ with energy splitting Δ and transition dipole moment μ is

[11] For instance $T_2 = 2T_1$ for pure radiative damping.

$$H = \begin{pmatrix} \frac{\Delta}{2} & -\mu E \mathrm{e}^{-\mathrm{i}\omega_f t} \\ -\mu E \mathrm{e}^{\mathrm{i}\omega_f t} & -\frac{\Delta}{2} \end{pmatrix}. \tag{21.240}$$

The corresponding magnetic field

$$B_x = \frac{2}{\gamma\hbar}\mu E \cos\omega_f t \tag{21.241}$$

$$B_y = \frac{2}{\gamma\hbar}\mu E \sin\omega_f t \tag{21.242}$$

$$B_z = -\frac{\Delta}{\gamma\hbar} \tag{21.243}$$

is that of a typical NMR experiment with a constant component along the z-axis and a rotating component in the xy-plane.

21.4.5.1 Free Precession

Consider the special case $B_z = \text{const.}$, $B_x = B_y = 0$. The corresponding Hamiltonian matrix is diagonal

$$H = \begin{pmatrix} \frac{\hbar\Omega_0}{2} & 0 \\ 0 & -\frac{\hbar\Omega_0}{2} \end{pmatrix} \tag{21.244}$$

with the Larmor-frequency

$$\Omega_0 = \frac{\Delta}{\hbar} = -\gamma B_0. \tag{21.245}$$

The equations of motion for the density matrix are

$$\frac{\partial}{\partial t}(\rho_{11} - \rho_{22}) = -\frac{(\rho_{11} - \rho_{22}) - (\rho_{11}^{eq} - \rho_{22}^{eq})}{T_1} \tag{21.246}$$

$$\mathrm{i}\hbar\frac{\partial}{\partial t}\rho_{12} = \hbar\Omega_0\rho_{12} - \mathrm{i}\hbar\frac{1}{T_2}\rho_{12} \tag{21.247}$$

with the solution

$$(\rho_{11} - \rho_{22}) = \left(\rho_{11}^{eq} - \rho_{22}^{eq}\right) + \left[\left(\rho_{11}(0) - \rho_{22}(0)\right) - \left(\rho_{11}^{eq} - \rho_{22}^{eq}\right)\right]\mathrm{e}^{-t/T_1} \tag{21.248}$$

$$\rho_{12} = \rho_{12}(0)\mathrm{e}^{-\mathrm{i}\Omega_0 t - t/T_2}. \tag{21.249}$$

The Bloch vector

$$\mathbf{r} = \begin{pmatrix} (x_0\cos\Omega_0 t - y_0\sin\Omega_0 t)\mathrm{e}^{-t/T_2} \\ (y_0\cos\Omega_0 t + x_0\sin\Omega_0 t)\mathrm{e}^{-t/T_2} \\ z^{eq} + (z_0 - z^{eq})\mathrm{e}^{-t/T_1} \end{pmatrix} \tag{21.250}$$

is subject to damped precession around the z-axis with the Larmor frequency (Fig. 21.20).

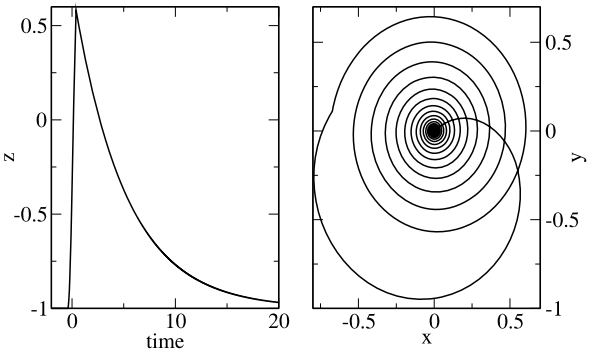

Fig. 21.20 (Free precession) The Bloch equations (21.239) are numerically solved with the 4th order Runge-Kutta method. After excitation with a short resonant pulse the free precession is observed. *Left*: The occupation difference $z = \rho_{11} - \rho_{22}$ decays exponentially to its equilibrium value. *Right*: In the xy-plane the Bloch vector moves on a spiral towards the equilibrium position ($x = 0$, $y = 0$)

21.4.5.2 Stationary Solution for Monochromatic Excitation

For the two-state system (21.240) with

$$H_{11} - H_{22} = \Delta = \hbar\Omega_0 \tag{21.251}$$

$$H_{12} = V_0(\cos\omega_f t - \mathrm{i}\sin\omega_f t) \tag{21.252}$$

the solution of the Bloch equations (21.238)

$$\frac{\mathrm{d}}{\mathrm{d}t}\begin{pmatrix} x \\ y \\ z \end{pmatrix} = \begin{pmatrix} -1/T_2 & -\Omega_0 & \frac{2V_0}{\hbar}\sin\omega_f t \\ \Omega_0 & -1/T_2 & -\frac{2V_0}{\hbar}\cos\omega_f t \\ -\frac{2V_0}{\hbar}\sin\omega_f t & \frac{2V_0}{\hbar}\cos\omega_f t & -1/T_1 \end{pmatrix}\begin{pmatrix} x \\ y \\ z \end{pmatrix} + \begin{pmatrix} 0 \\ 0 \\ z_{eq}/T_1 \end{pmatrix} \tag{21.253}$$

can be found explicitly [280]. We transform to a coordinate system which rotates around the z-axis ((13.3) on page 243) with angular velocity ω_f

$$\begin{pmatrix} x' \\ y' \\ z' \end{pmatrix} = \begin{pmatrix} \cos(\omega_f t) & \sin(\omega_f t) & 0 \\ -\sin(\omega_f t) & \cos(\omega_f t) & 0 \\ 0 & 0 & 1 \end{pmatrix}\begin{pmatrix} x \\ y \\ z \end{pmatrix} = A(t)\begin{pmatrix} x \\ y \\ z \end{pmatrix}. \tag{21.254}$$

Then

$$\frac{d}{dt}\begin{pmatrix} x' \\ y' \\ z' \end{pmatrix} = \dot{A}\begin{pmatrix} x \\ y \\ z \end{pmatrix} + A\frac{d}{dt}\begin{pmatrix} x \\ y \\ z \end{pmatrix} = \left(\dot{A}A^{-1} + AKA^{-1}\right)\begin{pmatrix} x' \\ y' \\ z' \end{pmatrix} + A\begin{pmatrix} 0 \\ 0 \\ \frac{z_{eq}}{T_1} \end{pmatrix} \tag{21.255}$$

with

$$K = \begin{pmatrix} -1/T_2 & -\Omega_0 & \frac{2V_0}{\hbar}\sin\omega_f t \\ \Omega_0 & -1/T_2 & -\frac{2V_0}{\hbar}\cos\omega_f t \\ -\frac{2V_0}{\hbar}\sin\omega_f t & \frac{2V_0}{\hbar}\cos\omega_f t & -1/T_1 \end{pmatrix}. \tag{21.256}$$

The matrix products are

$$\dot{A}A^{-1} = W = \begin{pmatrix} 0 & \omega_f & 0 \\ -\omega_f & 0 & 0 \\ 0 & 0 & 0 \end{pmatrix} \qquad AKA^{-1} = \begin{pmatrix} -1/T_2 & -\Omega_0 & 0 \\ \Omega_0 & -1/T_2 & -\frac{2V_0}{\hbar} \\ 0 & \frac{2V_0}{\hbar} & -1/T_1 \end{pmatrix} \tag{21.257}$$

and the equation of motion simplifies to

$$\begin{pmatrix} \dot{x}' \\ \dot{y}' \\ \dot{z}' \end{pmatrix} = \begin{pmatrix} -\frac{1}{T_2} & \omega_f - \Omega_0 & 0 \\ \Omega_0 - \omega_f & -\frac{1}{T_2} & -\frac{2V_0}{\hbar} \\ 0 & \frac{2V_0}{\hbar} & -\frac{1}{T_1} \end{pmatrix} \begin{pmatrix} x' \\ y' \\ z' \end{pmatrix} + \begin{pmatrix} 0 \\ 0 \\ \frac{z^{eq}}{T_1} \end{pmatrix}. \tag{21.258}$$

For times short compared to the relaxation times the solution is approximately given by harmonic oscillations. The generalized Rabi frequency Ω_R follows from [96]

$$\mathrm{i}\Omega_R x' = (\omega_f - \Omega_0)y' \tag{21.259}$$

$$\mathrm{i}\Omega_R y' = (\Omega_0 - \omega_f)x' - \frac{2V_0}{\hbar}z' \tag{21.260}$$

$$\mathrm{i}\Omega_R z' = \frac{2V_0}{\hbar}y' \tag{21.261}$$

as

$$\Omega_R = \sqrt{(\Omega_0 - \omega_f)^2 + \left(\frac{2V_0}{\hbar}\right)^2}. \tag{21.262}$$

At larger times these oscillations are damped and the stationary solution is approached (Fig. 21.21) which is given by

$$\frac{z^{eq}}{1 + 4\frac{V_0^2}{\hbar^2}T_1T_2 + T_2^2(\omega_f - \Omega_0)^2} \begin{pmatrix} 2T_2^2\frac{V_0}{\hbar}(\Omega_0 - \omega_f) \\ -2T_2\frac{V_0}{\hbar} \\ 1 + T_2^2(\omega_f - \Omega_0)^2 \end{pmatrix}. \tag{21.263}$$

The occupation difference

$$z = \rho_{11} - \rho_{22} = z^{eq}\left(1 - \frac{4\frac{V_0^2}{\hbar^2}T_1T_2}{1 + 4\frac{V_0^2}{\hbar^2}T_1T_2 + T_2^2(\omega_f - \Omega_0)^2}\right) \tag{21.264}$$

has the form of a Lorentzian. The line width increases for higher intensities (power broadening)

$$\Delta\omega = \frac{1}{T_2}\sqrt{1 + 4\frac{V_0^2}{\hbar^2}T_1T_2} \tag{21.265}$$

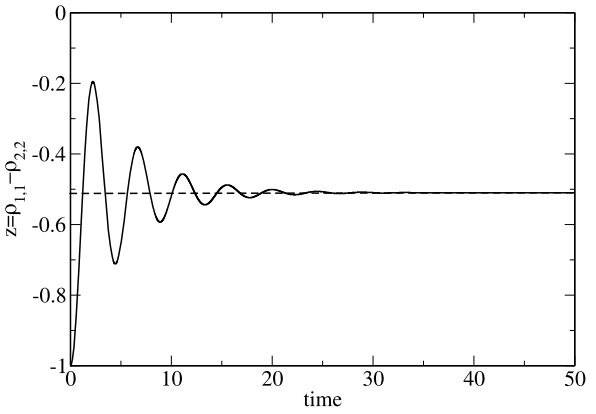

Fig. 21.21 (Monochromatic Excitation) The Bloch equations are solved numerically with the 4th order Runge-Kutta method for a monochromatic perturbation with $\omega = 4$, $V_0 = 0.5$. Parameters of the two-state system are $\omega_0 = 5$, $z_{eq} = -1.0$ and $T_1 = T_2 = 5.0$. The occupation difference $z = \rho_{11} - \rho_{22}$ initially shows Rabi oscillations which disappear at larger times where the stationary value $z = -0.51$ is reached

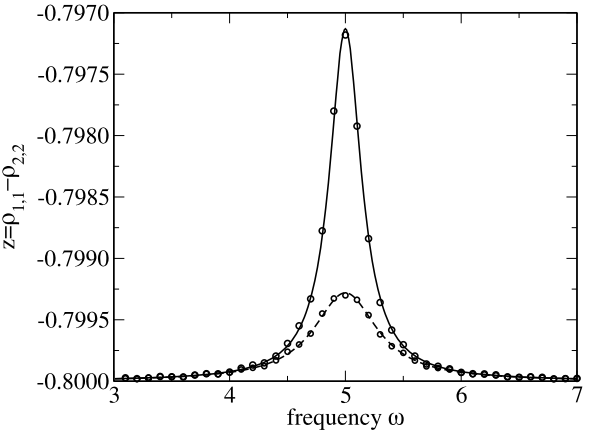

Fig. 21.22 (Resonance line) The equations of motion of the two-state system including relaxation terms are integrated with the 4th order Runge-Kutta method until a steady state is reached. Parameters are $\omega_0 = 5$, $z_{eq} = -0.8$, $V = 0.01$ and $T_1 = T_2 = 3.0, 6.9$. The change of the occupation difference is shown as a function of frequency (*circles*) and compared with the steady state solution (21.263)

and the maximum

$$\frac{z(\Omega_0)}{z^{eq}} = \frac{1}{1 + 4\frac{V_0^2}{\hbar^2} T_1 T_2} \tag{21.266}$$

approaches zero (saturation), Figs. 21.22, 21.23.

21.4.5.3 Excitation by a Resonant Pulse

For a resonant pulse with real valued envelope $V_0(t)$ and initial phase angle Φ_0

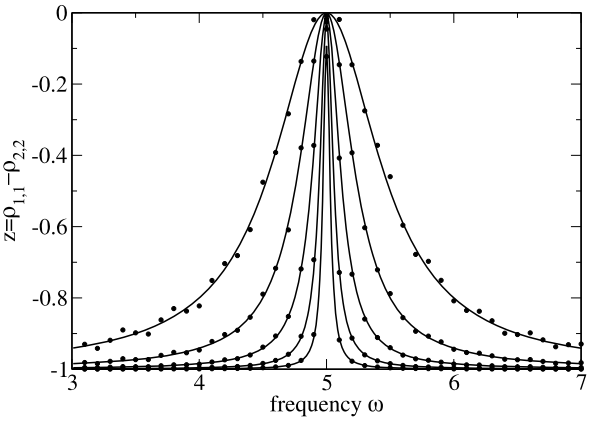

Fig. 21.23 (Power saturation and broadening) The resonance line is investigated as a function of the coupling strength V and compared with the stationary solution (21.263) to observe the broadening of the line width (21.265). Parameters are $\omega_0 = 5$, $z_{eq} = -1.0$, $T_1 = T_2 = 100$ and $V = 0.5$, 0.25, 0.125, 0.0625, 0.03125

$$H_{12} = V_0(t)\mathrm{e}^{-\mathrm{i}(\Omega_0 t+\Phi_0)}$$

the equation of motion in the rotating system is

$$\begin{pmatrix} \dot{x}' \\ \dot{y}' \\ \dot{z}' \end{pmatrix} = \begin{pmatrix} -\frac{1}{T_2} & 0 & -\frac{2V_0(t)}{\hbar}\sin\Phi_0 \\ 0 & -\frac{1}{T_2} & -\frac{2V_0(t)}{\hbar}\cos\Phi_0 \\ \frac{2V_0(t)}{\hbar}\sin\Phi_0 & \frac{2V_0(t)}{\hbar}\cos\Phi_0 & -\frac{1}{T_1} \end{pmatrix} \begin{pmatrix} x' \\ y' \\ z' \end{pmatrix} + \begin{pmatrix} 0 \\ 0 \\ \frac{z^{eq}}{T_1} \end{pmatrix}. \tag{21.267}$$

If the relaxation times are large compared to the pulse duration this describes approximately a rotation around an axis in the xy-plane (compare with (13.24))

$$\frac{\mathrm{d}}{\mathrm{d}t}\mathbf{r}' \approx W(t)\mathbf{r}' = \frac{2V_0(t)}{\hbar}W_0\mathbf{r}' \tag{21.268}$$

$$W_0 = \begin{pmatrix} 0 & 0 & -\sin\Phi_0 \\ 0 & 0 & -\cos\Phi_0 \\ \sin\Phi_0 & \cos\Phi_0 & 0 \end{pmatrix}. \tag{21.269}$$

Since the axis is time independent, a formal solution is given by

$$\mathbf{r}'(t) = \mathrm{e}^{W\int_{t_0}^{t}\frac{2V_0(t')}{\hbar}dt'}\mathbf{r}'(0) = \mathrm{e}^{W_0\Phi(t)}\mathbf{r}'(0) \tag{21.270}$$

with the phase angle

$$\Phi(t) = \int_{t_0}^{t}\frac{2V_0(t')}{\hbar}dt'. \tag{21.271}$$

Now, since

$$W_0^2 = \begin{pmatrix} -\sin^2\Phi_0 & -\sin\Phi_0\cos\Phi_0 & 0 \\ -\sin\Phi_0\cos\Phi_0 & -\cos^2\Phi_0 & 0 \\ 0 & 0 & -1 \end{pmatrix} \tag{21.272}$$

$$W_0^3 = -W_0 \tag{21.273}$$

$$W_0^4 = -W_0^2 \tag{21.274}$$

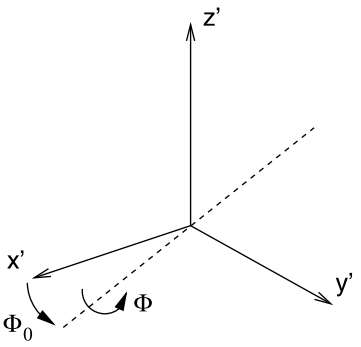

Fig. 21.24 (Rotation of the Bloch vector by a resonant pulse) A resonant pulse rotates the Bloch vector by the angle Φ around an axis in the $x'y'$-plane

the Taylor series of the exponential function in (21.270) can be summed up

$$
\begin{aligned}
&\mathrm{e}^{W_0\Phi} \\
&= 1 + \Phi W_0 + \frac{1}{2}\Phi^2 W_0^2 + \frac{1}{3!}\Phi^3 W_0^3 + \cdots \\
&= 1 + W_0^2\left(\frac{\Phi^2}{2} - \frac{\Phi^4}{4!} + \cdots\right) + W_0\left(\Phi - \frac{\Phi^3}{3!} + \cdots\right) \\
&= 1 + W_0^2(1 - \cos\Phi) + W_0 \sin\Phi \\
&= \begin{pmatrix} 1 - \sin^2\Phi_0(1-\cos\Phi) & -\sin\Phi_0\cos\Phi_0(1-\cos\Phi) & -\sin\Phi_0\sin\Phi \\ -\sin\Phi_0\cos\Phi_0(1-\cos\Phi) & 1 - \cos^2\Phi_0(1-\cos\Phi) & -\cos\Phi_0\sin\Phi \\ \sin\Phi_0\sin\Phi & \cos\Phi_0\sin\Phi & \cos\Phi \end{pmatrix} \\
&= \begin{pmatrix} \cos\Phi_0 & \sin\Phi_0 & 0 \\ -\sin\Phi_0 & \cos\Phi_0 & 0 \\ 0 & 0 & 1 \end{pmatrix} \begin{pmatrix} 1 & 0 & 0 \\ 0 & \cos\Phi & -\sin\Phi \\ 0 & \sin\Phi & \cos\Phi \end{pmatrix} \\
&\quad \times \begin{pmatrix} \cos\Phi_0 & -\sin\Phi_0 & 0 \\ \sin\Phi_0 & \cos\Phi_0 & 0 \\ 0 & 0 & 1 \end{pmatrix}. \qquad (21.275)
\end{aligned}
$$

The result is a rotation about the angle Φ around an axis in the xy-plane determined by Φ_0 (Fig. 21.24), especially around the x-axis for $\Phi_0 = 0$ and around the y-axis for $\Phi_0 = \frac{\pi}{2}$.

After a π-pulse ($\Phi = \pi$) the z-component changes its sign

$$
\mathbf{r}' = \begin{pmatrix} \cos(2\Phi_0) & -\sin(2\Phi_0) & 0 \\ -\sin(2\Phi_0) & -\cos(2\Phi_0) & 0 \\ 0 & 0 & -1 \end{pmatrix} \mathbf{r}(0). \qquad (21.276)
$$

The transition between the two basis states $z = -1$ and $z = 1$ corresponds to a spin flip (Fig. 21.25). On the other hand, a $\pi/2$-pulse transforms the basis states into a coherent mixture

$$
\mathbf{r}' = \begin{pmatrix} 1 - \sin^2\Phi_0 & -\sin\Phi_0\cos\Phi_0 & -\sin\Phi_0 \\ -\sin\Phi_0\cos\Phi_0 & 1 - \cos^2\Phi_0 & -\cos\Phi_0 \\ \sin\Phi_0 & \cos\Phi_0 & 0 \end{pmatrix} \mathbf{r}(0). \qquad (21.277)
$$

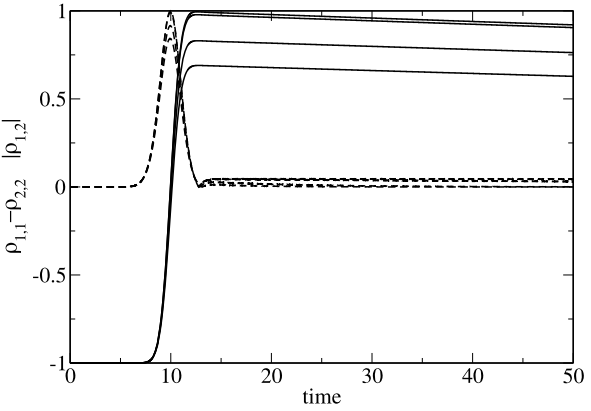

Fig. 21.25 (Spin flip by a π-pulse) The equations of motion of the Bloch vector (21.253) are solved with the 4th order Runge-Kutta method for an interaction pulse with a Gaussian shape. The pulse is adjusted to obtain a spin flip. The influence of dephasing processes is studied. $T_1 = 1000$, $t_p = 1.8$, $V_0 = 0.25$. The occupation difference $\rho_{11} - \rho_{22} = z$ (*solid curves*) and the coherence $|\rho_{12}| = \frac{1}{2}\sqrt{x^2 + y^2}$ (*broken curves*) are shown for several values of the dephasing time $T_2 = 5$, 10, 100, 1000

21.4.6 Elementary Qubit Manipulation

Whereas a classical bit can be only in one of two states

$$\text{either} \begin{pmatrix} 1 \\ 0 \end{pmatrix} \quad \text{or} \begin{pmatrix} 0 \\ 1 \end{pmatrix} \tag{21.278}$$

the state of a qubit is a quantum mechanical superposition

$$|\psi\rangle = C_0 \begin{pmatrix} 1 \\ 0 \end{pmatrix} + C_1 \begin{pmatrix} 0 \\ 1 \end{pmatrix}. \tag{21.279}$$

The time evolution of the qubit is described by a unitary transformation

$$|\psi\rangle \to U|\psi\rangle \tag{21.280}$$

which is represented by a complex 2×2 unitary matrix that has the general form (see also Sect. 13.14)

$$U = \begin{pmatrix} \alpha & \beta \\ -\mathrm{e}^{\mathrm{i}\varphi}\beta^* & \mathrm{e}^{\mathrm{i}\varphi}\alpha^* \end{pmatrix} \quad |\alpha|^2 + |\beta|^2 = 1, \quad \det U = \mathrm{e}^{\mathrm{i}\varphi}. \tag{21.281}$$

The Bloch vector is transformed with an orthogonal matrix A, which can be found from (21.212) and the transformed density matrix $U\rho U^{-1}$

$$\mathbf{r} \to A\mathbf{r} \quad A = \begin{pmatrix} \Re((\alpha^2 - \beta^2)\mathrm{e}^{-\mathrm{i}\varphi}) & \Im((\alpha^2 + \beta^2)\mathrm{e}^{-\mathrm{i}\varphi}) & -2\Re(\alpha\beta\mathrm{e}^{-\mathrm{i}\varphi}) \\ \Im((\beta^2 - \alpha^2)\mathrm{e}^{-\mathrm{i}\varphi}) & \Re((\alpha^2 + \beta^2)\mathrm{e}^{-\mathrm{i}\varphi}) & 2\Im(\alpha\beta\mathrm{e}^{-\mathrm{i}\varphi}) \\ 2\Re(\alpha^*\beta) & 2\Im(\alpha^*\beta) & (|\alpha|^2 - |\beta|^2) \end{pmatrix}. \tag{21.282}$$

Any single qubit transformation can be realized as a sequence of rotations around just two axes [126, 183, 263]. In the following we consider some simple transformations, so called quantum gates [274].

21.4.6.1 Pauli-Gates

Of special interest are the gates represented by the Pauli matrices $U = \sigma_i$ since any complex 2×2 matrix can be obtained as a linear combination of the Pauli matrices and the unit matrix (Sect. 13.14). For all three of them $\det U = -1$ and $\varphi = \pi$.

The X-gate

$$U_X = \sigma_x = \begin{pmatrix} 0 & 1 \\ 1 & 0 \end{pmatrix} \tag{21.283}$$

corresponds to rotation by π radians around the x-axis ((21.276) with $\Phi_0 = 0$)

$$A_X = \begin{pmatrix} 1 & 0 & 0 \\ 0 & -1 & 0 \\ 0 & 0 & -1 \end{pmatrix}. \tag{21.284}$$

It is also known as NOT-gate since it exchanges the two basis states. Similarly, the Y-gate

$$U_Y = \sigma_y = \begin{pmatrix} 0 & -i \\ i & 0 \end{pmatrix}$$

rotates the Bloch vector by π radians around the y-axis (21.276 with $\Phi_0 = \pi/2$)

$$A_Y = \begin{pmatrix} -1 & 0 & 0 \\ 0 & 1 & 0 \\ 0 & 0 & -1 \end{pmatrix} \tag{21.285}$$

and the Z-gate

$$U_Z = \sigma_z = \begin{pmatrix} 1 & 0 \\ 0 & -1 \end{pmatrix} \tag{21.286}$$

by π radians around the z-axis

$$A_Z = \begin{pmatrix} -1 & 0 & 0 \\ 0 & -1 & 0 \\ 0 & 0 & 1 \end{pmatrix}. \tag{21.287}$$

This rotation can be replaced by two successive rotations in the xy-plane

$$A_Z = A_X A_Y. \tag{21.288}$$

The corresponding transformation of the wavefunction produces an overall phase shift of $\pi/2$ since the product of the Pauli matrices is $\sigma_x \sigma_y = \mathrm{i}\sigma_z$, which is not relevant for observable quantities.

21.4.6.2 Hadamard Gate

The Hadamard gate is a very important ingredient for quantum computation. It transforms the basis states into coherent superpositions and vice versa. It is described by the matrix

$$U_H = \begin{pmatrix} \frac{1}{\sqrt{2}} & \frac{1}{\sqrt{2}} \\ \frac{1}{\sqrt{2}} & -\frac{1}{\sqrt{2}} \end{pmatrix} \tag{21.289}$$

with $\det U_H = -1$ and

$$A_H = \begin{pmatrix} 0 & 0 & 1 \\ 0 & -1 & 0 \\ 1 & 0 & 0 \end{pmatrix} \tag{21.290}$$

which can be obtained as the product

$$A_H = \begin{pmatrix} 0 & 0 & -1 \\ 0 & 1 & 0 \\ 1 & 0 & 0 \end{pmatrix} \begin{pmatrix} 1 & 0 & 0 \\ 0 & -1 & 0 \\ 0 & 0 & -1 \end{pmatrix} \tag{21.291}$$

of a rotation by π radians around the x-axis and a second rotation by $\pi/2$ radians around the y-axis. The first rotation corresponds to the X-gate and the second to (21.277) with $\Phi_0 = \pi/2$

$$U = \begin{pmatrix} \frac{1}{\sqrt{2}} & \frac{1}{\sqrt{2}} \\ -\frac{1}{\sqrt{2}} & \frac{1}{\sqrt{2}} \end{pmatrix}. \tag{21.292}$$

21.5 Problems

Problem 21.1 (Wave packet motion) In this computer experiment we solve the Schrödinger equation for a particle in the potential $V(x)$ for an initially localized Gaussian wave packet $\psi(t = 0, x) \sim \exp(-a(x - x_0)^2)$. The potential is a box, a harmonic parabola or a fourth order double well. Initial width and position of the wave packet can be varied.

- Try to generate the time independent ground state wave function for the harmonic oscillator.
- Observe the dispersion of the wave packet for different conditions and try to generate a moving wave packet with little dispersion.
- Try to observe tunneling in the double well potential.

Problem 21.2 (Two-state system) In this computer experiment a two-state system is simulated. Amplitude and frequency of an external field can be varied as well as the energy gap between the two states (see Fig. 21.9).

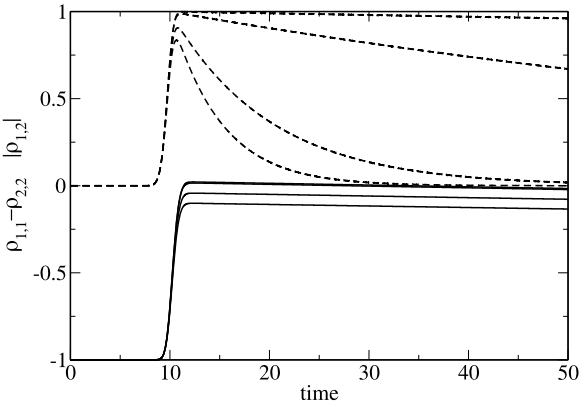

Fig. 21.26 (Generation of a coherent mixture by a $\pi/2$-pulse) The equations of motion of the Bloch vector (21.253) are solved with the 4th order Runge-Kutta method for an interaction pulse with a Gaussian shape. The pulse is adjusted to obtain a coherent mixture. The influence of dephasing processes is studied. $T_1 = 1000$, $t_p = 0.9$, $V_0 = 0.25$. The occupation difference $\rho_{11} - \rho_{22} = z$ (*solid curves*) and the coherence $|\rho_{12}| = \frac{1}{2}\sqrt{x^2 + y^2}$ (*broken curves*) are shown for several values of the dephasing time $T_2 = 5$, 10, 100, 1000

- Compare the time evolution at resonance and away from it.

Problem 21.3 (Three-state system) In this computer experiment a three-state system is simulated.

- Verify that the system behaves like an effective two-state system if the intermediate state is higher in energy than initial and final states (see Fig. 21.13).

Problem 21.4 (Ladder model) In this computer experiment the ladder model is simulated. The coupling strength and the spacing of the final states can be varied.

- Check the validity of the exponential decay approximation (see Fig. 21.15).

Problem 21.5 (Landau-Zener model) This computer experiment simulates the Landau Zener model. The coupling strength and the nuclear velocity can be varied (see Fig. 21.18).

- Try to find parameters for an efficient crossing of the states.

Problem 21.6 (Resonance line) In this computer experiment a two-state system with damping is simulated. The resonance curve is calculated from the steady state occupation probabilities (see Figs. 21.22, 21.23).

- Study the dependence of the line width on the intensity (power broadening).

Problem 21.7 (Spin flip) The damped two-state system is now subject to an external pulsed field (see Figs. 21.25, 21.26, 21.27).

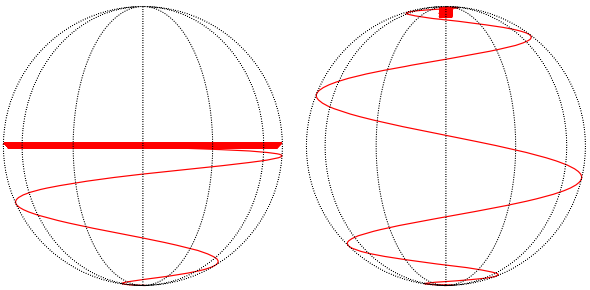

Fig. 21.27 (Motion of the Bloch vector during $\frac{\pi}{2}$ and π pulses) The trace of the Bloch vector is shown in the laboratory system. *Left*: $\frac{\pi}{2}$-pulse as in Fig. 21.26 with $T_2 = 1000$. *Right*: π-pulse as in Fig. 21.25 with $T_2 = 1000$

- Try to produce a coherent superposition state ($\pi/2$ pulse) or a spin flip (π pulse).
- Investigate the influence of decoherence.